

# Phonon-induced decoherence for a quantum dot spin qubit operated by Raman passage

K. Roszak,<sup>1</sup> A. Grodecka,<sup>1</sup> P. Machnikowski,<sup>1,2,\*</sup> and T. Kuhn<sup>2</sup>

<sup>1</sup>*Institute of Physics, Wrocław University of Technology, 50-370 Wrocław, Poland*

<sup>2</sup>*Institut für Festkörperteorie, Westfälische Wilhelms-Universität, 48149 Münster, Germany*

We study single-qubit gates performed via stimulated Raman adiabatic passage (STIRAP) on a spin qubit implemented in a quantum dot system in the presence of phonons. We analyze the interplay of various kinds of errors resulting from the carrier-phonon interaction (including also the effects of spin-orbit coupling) as well as from quantum jumps related to nonadiabaticity and calculate the fidelity as a function of the pulse parameters. We give quantitative estimates for an InAs/GaAs system and identify the parameter values for which the error is considerably minimized, even to values below  $10^{-4}$  per operation.

PACS numbers: 03.67.Lx, 03.65.Yz, 63.20.Kr, 42.50.Hz

## I. INTRODUCTION

Quantum dots (QDs), among many other systems,<sup>1</sup> are considered to be promising candidates for an implementation of quantum information processing schemes. Due to their atomic-like structure<sup>2</sup> one can easily single out a subset of states to encode the logical qubit values. In principle, these systems provide for stable coherent memory if the information is encoded into the long-living electron spin,<sup>3</sup> which motivated a spin-based proposal for quantum information storage and processing.<sup>4</sup> On the other hand, experimental demonstrations of coherent control over the charge (orbital) degrees of freedom<sup>5,6,7,8,9</sup> and the recently performed two-qubit gate based on a confined biexciton system<sup>10</sup> prove the feasibility of quantum coherent manipulation of carrier states on picosecond time scales. It has been therefore proposed<sup>11</sup> to implement the qubit states as the vacuum and single exciton states in a QD, switched by resonant optical coupling and providing the two-qubit conditional gating via inter-QD dipole-dipole interaction.

Both the spin-based and the charge-based proposals suffer from serious difficulties. The spin switching time in typical structures is very long due to weak magnetic coupling. The orbital degrees of freedom do not provide for long operation times due to the finite exciton lifetime, usually of order of 1 ns.<sup>12,13</sup> It seems therefore natural to seek for a scheme in which the logical values are stored using spin states, while the operations are performed via optical coupling to the charge degrees of freedom<sup>14,15</sup>, also using QD systems in QED cavities.<sup>16,17</sup>

A promising solution, proposed recently,<sup>18</sup> is to encode the qubit states into spin states of an excess electron in a QD and perform operations by employing the stimulated Raman adiabatic passage (STIRAP) to a state localized spatially in a neighboring dot.<sup>19</sup> (An alternative scheme not relying on the auxiliary state has also been proposed<sup>20</sup>). The STIRAP technique uses three laser fields that couple the two qubit states as well as the auxiliary state to a fourth state, a charged exciton ( $X^-$ , or trion), composed of two electrons with oppo-

site spins and a hole. In the presence of laser fields with slowly varying amplitudes, the system evolves adiabatically, following the states of the interacting system of carriers and electromagnetic field (trapped states). The driving fields may be chosen in such a way that the trion state is never occupied (in the ideal case) so that the scheme is not affected by the decoherence resulting from its finite lifetime. It can be shown<sup>21</sup> that with properly chosen phases of the laser pulses a pre-defined qubit superposition gets coupled and undergoes an adiabatic transition to the second dot and back which shifts its phase by a desired angle with respect to the other, orthogonal superposition that remains decoupled from the laser fields. This results in an arbitrary rotation of the qubit state around an arbitrary axis on the qubit Bloch sphere.

The essential difference between the atomic systems, where such quantum-optical schemes are successfully applied,<sup>22</sup> and the solid state QD systems, where their new implementation is proposed, is the nature of the environment. In high-quality samples at low temperatures the dominant coupling to the external degrees of freedom is that involving lattice modes (phonons). The coupling mechanisms include interaction with lattice polarization (longitudinal optical, LO, phonons) and with piezoelectric fields induced by phonon-related strain (longitudinal and transverse acoustic, LA and TA, phonons) as well as the effective influence of strain-induced band shift, described in terms of the deformation potential coupling to LA phonons. Even restricted to acoustic phonons, this kind of external bath shows various peculiarities compared to models usually assumed in general studies.<sup>23</sup> Its low-frequency behavior depends on the coupling mechanism and on the wave-function geometry and is always super-ohmic, i.e., its spectral density grows super-linearly with frequency.<sup>24</sup> Due to the localization of carrier wave-functions on a scale much larger than the lattice constant, a high-frequency exponential cut-off in the effective phonon spectral densities appears well below the Debye frequency. Moreover, apart from the non-diagonal coupling terms describing real transi-

tions, there is usually a diagonal coupling which leads to pure dephasing effects<sup>24,25</sup> resulting from the lattice relaxation after a fast (compared to phonon frequencies) change of the carrier state.<sup>25,26</sup> Such an effect manifests itself in optical experiments as a fast partial decay of the signal coherence<sup>9,12</sup> in excellent agreement with theoretical modeling assuming its phonon-related origin.<sup>27,28</sup>

The characteristic time scales of these intrinsically non-Markovian pure dephasing processes are determined by the localization (QD size) and are typically much shorter than any real phonon-induced transition process. More importantly, they overlap with the time scales proposed for optical qubit control.<sup>11</sup> It has been shown<sup>29</sup> that the demand to avoid these pure dephasing effects limits from *below* the gating times, thus shrinking the time scale window defined, on the other side, by the long-time decoherence processes (e.g. the exciton lifetime).

In this paper we study the influence of the coupling to the phonon degrees of freedom on the fidelity of the single qubit rotation via the STIRAP process<sup>21</sup> implemented in the double-QD structure.<sup>18</sup> Even if the possible phonon-assisted transitions to other states may be neglected, the diagonal terms still give rise not only to pure dephasing effects but also to transitions between the trapped carrier-field states. The probability of these phonon-induced transitions becomes very high if the spacing between the trapped energy levels falls into the area of high phonon spectral density and the overall error is roughly proportional to the process duration. Such high error rates are critical for quantum computation schemes where extremely high fidelity is required (e.g., errors not higher than  $\sim 10^{-4}$  per gate are allowed for two-qubit operations) in order to provide for scalable devices including quantum error correction schemes. We discuss how these strong decoherence processes may be avoided by either decreasing the trapped level separation (low-frequency regime, exploiting the super-ohmic behavior of spectral densities) or increasing it beyond the cut-off (high frequency regime). We show that in both cases one encounters a trade-off situation, due to the opposite requirements for phonon-induced jumps (short duration) and for the fundamental adiabaticity condition and pure dephasing (slow operation): In the low-frequency regime, avoiding phonon-induced transitions contradicts the condition for avoiding nonadiabatic jumps between the trapped states, which may be overcome only by considerably extending the process duration. In the high-frequency case, there is a competition between the pure dephasing and the phonon-induced transitions that is overcome by increasing the trapped state splitting, taking advantage of the particular structure of the phonon spectral density for a double dot structure.

The paper is organized as follows. In the next Section II we present the general derivation of the phonon-induced error for an arbitrary system evolution. The Section III describes the model of the specific system discussed in the paper and derives the carrier-phonon coupling relevant for our discussion. The Section IV provides

a description of the STIRAP qubit rotation procedure for completeness and necessary reference. In the central Section V, the results of Sec. II are applied to the STIRAP procedure described in Sec. IV with the phonon perturbation derived in Sec. III. This section contains also some general discussion. In the Section VI we present the results for specific pulse shapes in order to get some quantitative estimates for an InAs/GaAs QD system. Finally, the Section VII summarizes and concludes the paper. In addition, some technical details and further analysis, including the effect of the spin-orbit coupling, are presented in the Appendices.

## II. PHONON-INDUCED DECOHERENCE: GENERAL THEORY

Subject of this paper is the optically induced dynamics in a quantum dot structure coupled to a phonon bath. In this Section we derive the equations for the reduced density matrix of the carrier subsystem in the leading order in the phonon coupling, assuming that the unperturbed (ideal) evolution of the noninteracting system, described by the unitary evolution operator

$$U_0(t) = U_C(t) \otimes e^{-iH_{\text{ph}}t/\hbar} \quad (1)$$

is known (see also Ref. 30). Here,  $U_C$  is the evolution operator for the carrier subsystem coupled to the external light field in absence of carrier-phonon interaction and  $H_{\text{ph}}$  is the free phonon Hamiltonian. The relevant carrier states in the quantum dot are assumed to form a discrete set  $|n\rangle$ ,  $n = 0, 1, 2, \dots$ , and the phonons are described by destruction and creation operators  $b_{\mathbf{k}}$  and  $b_{\mathbf{k}}^\dagger$  referring to bulk phonon modes with wave vector  $\mathbf{k}$ .

The interaction between the carriers and the phonon modes is written in the general form

$$V = \sum_{nn'} S_{nn'} \otimes R_{nn'}, \quad (2)$$

where  $S_{nn'} = S_{n'n}^\dagger = |n\rangle\langle n'|$  act in the Hilbert space of the carrier subsystem and

$$R_{nn'} = R_{n'n}^\dagger = \sum_{\mathbf{k}} F_{nn'}(\mathbf{k}) (b_{\mathbf{k}} + b_{-\mathbf{k}}^\dagger), \quad (3)$$

with  $F_{nn'}(\mathbf{k}) = F_{n'n}^*(-\mathbf{k})$ , affect only the phonon environment.

We assume that at the initial time  $-t_0$  the system is in the product state

$$\varrho(-t_0) = \rho_0 \otimes \rho_T, \quad \rho_0 = |\psi_0\rangle\langle\psi_0|, \quad (4)$$

where  $|\psi_0\rangle$  is a certain state of the carrier subsystem and  $\rho_T$  is the thermal equilibrium distribution of phonon modes. Physically, this is justified by the existence of two distinct time scales: the long one for the carrier decoherence (e.g. about 1 ns ground state exciton lifetime<sup>12,13</sup>)

and the short one for the reservoir relaxation (1 ps pure dephasing time<sup>12,24,26</sup>).

The starting point is the evolution equation for the density matrix of the total system in the interaction picture with respect to the externally driven evolution  $U_0$ , in the second order Born approximation with respect to the carrier-phonon interaction<sup>31</sup>

$$\begin{aligned} \tilde{\varrho}(t) &= \tilde{\varrho}(-t_0) + \frac{1}{i\hbar} \int_{-t_0}^t d\tau [V(\tau), \varrho(-t_0)] \\ &\quad - \frac{1}{\hbar^2} \int_{-t_0}^t d\tau \int_{-t_0}^{\tau} d\tau' [V(\tau), [V(\tau'), \varrho(-t_0)]], \end{aligned} \quad (5)$$

where

$$\tilde{\varrho}(t) = U_0^\dagger(t) \varrho(t) U_0(t), \quad V(t) = U_0^\dagger(t) V U_0(t).$$

The reduced density matrix of the carrier subsystem is

$$\rho(t) = U_C(t) \tilde{\rho}(t) U_C^\dagger(t), \quad \tilde{\rho}(t) = [\text{Tr}_R \tilde{\varrho}(t)],$$

where the trace is taken over the reservoir degrees of freedom. Note that in this paper the symbol  $\varrho$  always refers to a density matrix in the full carrier-phonon Hilbert space while  $\rho$  refers to reduced density matrices either in the phonon or the carrier subspace. The first (zeroth order) term in (5) obviously yields

$$\rho^{(0)}(t) = U_C(t) |\psi_0\rangle \langle \psi_0| U_C^\dagger(t) = |\psi_0(t)\rangle \langle \psi_0(t)|. \quad (6)$$

The second term vanishes, since it contains the thermal average of an odd number of phonon operators. The third (second order) term describes the leading phonon correction to the dynamics of the carrier subsystem,

$$\begin{aligned} \tilde{\rho}^{(2)}(t) &= \\ &\quad - \frac{1}{\hbar^2} \int_{-t_0}^t d\tau \int_{-t_0}^{\tau} d\tau' \text{Tr}_R [V(\tau), [V(\tau'), \varrho(-t_0)]]. \end{aligned} \quad (7)$$

The first of the four terms resulting from expanding the commutators in (7) is  $-Q_t \rho_0$ , where

$$\begin{aligned} Q_t &= \frac{1}{\hbar^2} \sum_{nn'} \sum_{mm'} \int_{-t_0}^t d\tau \int_{-t_0}^{\tau} d\tau' \\ &\quad \times S_{nn'}(\tau) S_{mm'}(\tau') \langle R_{nn'}(\tau - \tau') R_{mm'} \rangle. \end{aligned}$$

The operators  $S$  and  $R$  are transformed into the interaction picture in the usual way

$$S_{nn'}(t) = U_0^\dagger(t) S_{nn'} U_0(t), \quad R_{nn'}(t) = U_0^\dagger(t) R_{nn'} U_0(t)$$

and  $\langle \hat{\mathcal{O}} \rangle = \text{Tr}_R [\hat{\mathcal{O}} \rho_T]$  denotes the thermal average (obviously  $[U_0(t), \rho_T] = 0$ ). Using the symmetry of the operators  $S_{nn'}$  and  $R_{nn'}$  the second term may be written as

$-\rho_0 Q_t^\dagger$ . In a similar manner, the two other terms may be combined to  $\hat{\Phi}_t[\rho_0]$ , where

$$\begin{aligned} \hat{\Phi}_t[\rho] &= \frac{1}{\hbar^2} \sum_{nn'} \sum_{mm'} \int_{-t_0}^t d\tau \int_{-t_0}^{\tau} d\tau' \\ &\quad \times S_{nn'}(\tau') \rho S_{mm'}(\tau) \langle R_{mm'}(\tau - \tau') R_{nn'} \rangle. \end{aligned}$$

In terms of the new hermitian operators

$$A_t = Q_t + Q_t^\dagger, \quad h_t = \frac{1}{2i} (Q_t - Q_t^\dagger), \quad (8)$$

the perturbation to the density matrix at the final time  $t$  (7) may be written as

$$\tilde{\rho}^{(2)}(t) = -i [h_t, \rho_0] - \frac{1}{2} \{A_t, \rho_0\} + \hat{\Phi}_t[\rho_0]. \quad (9)$$

The first term is a Hamiltonian correction which does not lead to irreversible effects and in principle may be compensated for by an appropriate modification of the control Hamiltonian  $H_C$ . The other two terms describe processes of entangling the system with the reservoir, leading to the loss of coherence of the carrier state.

Introducing the spectral density of the reservoir,

$$R_{nn',mm'}(\omega) = \frac{1}{2\pi\hbar^2} \int dt \langle R_{nn'}(t) R_{mm'} \rangle e^{i\omega t}, \quad (10)$$

one may write

$$\hat{\Phi}_t[\rho] = \sum_{nn'} \sum_{mm'} \int d\omega R_{nn',mm'}(\omega) Y_{mm'}(\omega) \rho Y_{nn'}^\dagger(\omega) \quad (11)$$

where the frequency-dependent operators have been introduced,

$$Y_{nn'}(\omega) = \int_{-t_0}^t S_{nn'}(\tau) e^{i\omega\tau} d\tau. \quad (12)$$

Using (10) one has also

$$\begin{aligned} Q_t &= \sum_{nn'} \sum_{mm'} \int d\omega \int_{-t_0}^t d\tau \int_{-t_0}^{\tau} d\tau' \Theta(\tau - \tau') \\ &\quad \times S_{nn'}(\tau) S_{mm'}(\tau') R_{nn',mm'}(\omega) e^{-i\omega(\tau - \tau')}. \end{aligned}$$

Next, representing the Heaviside function as

$$\Theta(t) = -e^{i\omega t} \int \frac{d\omega'}{2\pi i} \frac{e^{-i\omega't}}{\omega' - \omega + i0^+},$$

we write

$$\begin{aligned}
Q_t &= -\sum_{nn'} \sum_{mm'} \int d\omega R_{nn',mm'}(\omega) \int \frac{d\omega'}{2\pi i} \frac{Y_{n'n}^\dagger(\omega') Y_{mm'}(\omega')}{\omega' - \omega + i0^+} \\
&= -\sum_{nn'} \sum_{mm'} \int d\omega R_{nn',mm'}(\omega) \int \frac{d\omega'}{2\pi i} Y_{n'n}^\dagger(\omega') Y_{mm'}(\omega') \left[ -i\pi\delta(\omega' - \omega) + \mathcal{P} \frac{1}{\omega' - \omega} \right],
\end{aligned}$$

where  $\mathcal{P}$  denotes the principal value.

Hence, the two Hermitian operators defined in (8) take the form

$$A_t = \sum_{nn'} \sum_{mm'} \int d\omega R_{nn',mm'}(\omega) Y_{n'n}^\dagger(\omega) Y_{mm'}(\omega) \quad (13)$$

and

$$\begin{aligned}
h_t &= \sum_{nn'} \sum_{mm'} \int d\omega R_{nn',mm'}(\omega) \mathcal{P} \int \frac{d\omega'}{2\pi} \frac{Y_{n'n}^\dagger(\omega') Y_{mm'}(\omega')}{\omega' - \omega}.
\end{aligned} \quad (14)$$

In the following, we will be interested in the system state at the final time  $t = +t_0$ , after all the pulses have been switched off.

In the quantum information processing context it is customary to quantify the quality of the operation in terms of the fidelity, which is a measure of the overlap between the desired (unperturbed) state and the actual final state,  $F = \text{Tr}[U_C(t)\rho_0 U_C^\dagger(t)\rho(t)]$ . The error is then defined as the fidelity loss,  $\delta = 1 - F$ . From Eqs. (6) and (9) one has

$$\begin{aligned}
\delta &= -\langle \psi_0 | \tilde{\rho}^{(2)} | \psi_0 \rangle \\
&= \sum_{nn'mm'} \int d\omega R_{nn',mm'}(\omega) \\
&\quad \times \langle \psi_0 | Y_{n'n}^\dagger(\omega) \mathbf{P}^\perp Y_{mm'}(\omega) | \psi_0 \rangle,
\end{aligned} \quad (15)$$

where  $\mathbf{P}^\perp$  is the projector on the orthogonal complement of  $|\psi_0\rangle$  in the carrier space. In this order the unitary correction generated by  $h_t$  does not contribute to the error.

The calculation presented above requires two input components: the specific form of the interaction potential [Eq. (2)] for a given problem and the unperturbed time evolution [Eq. (1)]. These two necessary elements are derived for our qubit system in the two following sections.

### III. THE QUBIT SYSTEM AND ITS INTERACTION WITH PHONONS

In the following part of the paper, the general theory will be applied to a specific system of two quantum dots containing one excess electron and coupled to the trion

state in order to perform an arbitrary rotation in the qubit space by means of the STIRAP. Here we formulate the model of this system and derive the Hamiltonian describing its interaction with the phonon environment.

The Hamiltonian describing this system and its coupling to lattice modes may be written as

$$H = H_C + H_{\text{ph}} + V, \quad (16)$$

The first term is the STIRAP Hamiltonian including both the qubit states and the control fields. The implementation<sup>18</sup> defines the qubit by two  $\sigma_y$  spin eigenstates of a single excess electron in one of the QDs (“large”) from a vertically stacked pair. In order to perform a general single-qubit rotation between the two qubit states  $|0\rangle$  and  $|1\rangle$  an auxiliary state  $|2\rangle$  is used<sup>21</sup>, in which the electron is shifted to the second (“small”) dot and has the same spin orientation as in  $|0\rangle$ . All these three states are coupled to a fourth state  $|3\rangle$ , a charged exciton (trion) state, by laser beams  $\Omega_0, \Omega_1, \Omega_2$ , respectively. The Hamiltonian for such a system in rotating wave approximation (RWA) is

$$\begin{aligned}
H_C &= \sum_n \epsilon_n |n\rangle\langle n| \\
&\quad + \sum_{n=0}^2 \hbar\Omega_n(t) \left( e^{i(\omega_n t - \delta_n)} |n\rangle\langle 3| + \text{H.c.} \right),
\end{aligned} \quad (17)$$

where  $\epsilon_n$  are the energies of the corresponding states, the slowly varying pulse envelopes  $\Omega_n(t)$  are real and positive,  $\omega_n$  are the corresponding laser frequencies and  $\delta_n$  are the phases of the pulses. This Hamiltonian induces the unitary evolution described in the previous section by the operator  $U_C$  [Eq. (1)].

In order to achieve the Raman coupling, the frequencies  $\omega_n$  of the laser beams must be chosen such that the detunings from the corresponding dipole transition energies  $\epsilon_3 - \epsilon_n$  are the same for all the three couplings. Therefore, we put  $\omega_n = \epsilon_3/\hbar - \epsilon_n/\hbar - \Delta$ ,  $n = 0, 1, 2$ , where  $\Delta$ , the common detuning, is one of the parameters to be tuned for optimal performance. In the rotating frame, defined by  $|\tilde{n}\rangle = e^{i(\omega_n t - \delta_0)} |n\rangle$ ,  $n = 0, 1, 2$ , the RWA Hamiltonian (17) may be written

$$\begin{aligned}
H_C &= \hbar\Delta |3\rangle\langle 3| + \frac{1}{2} \sum_{n=0}^2 \hbar\Omega_n(t) \left( e^{-i\tilde{\delta}_n} |\tilde{n}\rangle\langle 3| + e^{i\tilde{\delta}_n} |3\rangle\langle \tilde{n}| \right),
\end{aligned} \quad (18)$$

where  $\tilde{\delta}_n = \delta_n - \delta_0$  (only the relative phase of the pulses matters).

The second term describes the free phonon evolution,

$$H_{\text{ph}} = \sum \hbar \omega_{\mathbf{k}} \beta_{\mathbf{k}}^\dagger \beta_{\mathbf{k}},$$

where  $\beta_{\mathbf{k}}^\dagger, \beta_{\mathbf{k}}$  are phonon creation and annihilation operators (with respect to the crystal ground state). Throughout the paper, the phonon branch index will be implicit in  $\mathbf{k}$ , unless it is explicitly written. Together with  $H_C$  [Eq. (17)], the above phonon Hamiltonian describes the known, unperturbed evolution of the system, given by Eq. (1).

The final term is the carrier-phonon interaction. Since the adiabaticity inherent in the STIRAP procedure excludes the possibility of inducing high-frequency dynamics and also all the trapped state splittings should be at most of several meV (to avoid crossing with excited carrier states), the discussion will be restricted to acoustic phonons. The Hamiltonian describing the electron-phonon interaction in the coordinate representation is

$$V = \sum_{\mathbf{k}} v_{\mathbf{k}} e^{i\mathbf{k}\cdot\mathbf{r}} \left( \beta_{\mathbf{k}} + \beta_{-\mathbf{k}}^\dagger \right), \quad (19)$$

where  $\mathbf{r}$  denotes the electron coordinate (a similar contribution appears for holes). The coupling constants for the longitudinal and transverse phonon branches are, respectively<sup>32,33</sup>,

$$v_{\mathbf{k}}^{(l)} = \sqrt{\frac{\hbar}{2\rho_c V_n \omega_l(\mathbf{k})}} \left[ \sigma k - i \frac{de}{\varepsilon_0 \varepsilon_s} M_l(\hat{\mathbf{k}}) \right], \quad (20a)$$

and

$$v_{\mathbf{k}}^{(t_1, t_2)} = -i \sqrt{\frac{\hbar}{2\rho_c V_n \omega_t(\mathbf{k})}} \frac{de}{\varepsilon_0 \varepsilon_s} M_{t_1, t_2}(\hat{\mathbf{k}}) \mathcal{F}_{nn'}(\mathbf{k}), \quad (20b)$$

where  $l, t_1, t_2$  refer to the longitudinal and two transverse acoustic phonon branches. Here  $e$  denotes the electron charge,  $\rho_c$  is the crystal density,  $V_n$  is the normalization volume of the phonon system,  $\omega_{l, t}$  are the phonon frequencies,  $d$  is the piezoelectric constant,  $\varepsilon_0$  is the vacuum dielectric constant,  $\varepsilon_s$  is the static relative dielectric constant and  $\sigma$  is the deformation potential constant for electrons. The functions  $M_s$  depend on the orientation of the phonon wave vector<sup>33</sup>. For the zinc-blende structure they are given by

$$M_s(\hat{\mathbf{k}}) = 2 \left[ \hat{k}_x \hat{k}_y (\hat{e}_{s, \mathbf{k}})_z + \hat{k}_y \hat{k}_z (\hat{e}_{s, \mathbf{k}})_x + \hat{k}_z \hat{k}_x (\hat{e}_{s, \mathbf{k}})_y \right], \quad (21)$$

where  $\hat{\mathbf{k}} = \mathbf{k}/k$  and  $\hat{e}_{s, \mathbf{k}}$  is the unit polarization vector for the wave vector  $\mathbf{k}$  and polarization  $s$ .

In the basis of the confined states relevant for the STIRAP process the carrier-phonon interaction Hamiltonian (19) reads

$$V = \sum_{n, n'=0}^3 |n\rangle\langle n'| \sum_{\mathbf{k}} f_{nn'}(\mathbf{k}) \left( \beta_{\mathbf{k}} + \beta_{-\mathbf{k}}^\dagger \right), \quad (22)$$

where, for single-electron states,  $f_{nn'}(\mathbf{k}) = v_{\mathbf{k}} \mathcal{F}_{nn'}(\mathbf{k})$  with the form factors  $\mathcal{F}_{nn'}(\mathbf{k})$  depending on the wave function geometry and given by

$$\mathcal{F}_{nn'}(\mathbf{k}) = \int d^3\mathbf{r} \Psi_n^*(\mathbf{r}) e^{i\mathbf{k}\cdot\mathbf{r}} \Psi_{n'}(\mathbf{r}), \quad (23)$$

where  $\Psi_n(\mathbf{r})$  is the envelope wave-function of the electron. The coupling constants  $f_{nn'}(\mathbf{k})$  include all the coupling mechanisms relevant for a given phonon branch and have the symmetry  $f_{nn'}(\mathbf{k}) = f_{n'n}^*(-\mathbf{k})$ .

We will assume that the two spin states used to encode  $|0\rangle$  and  $|1\rangle$  correspond to the same orbital wave-functions so that the couplings  $f_{00}(\mathbf{k})$  and  $f_{11}(\mathbf{k})$  are equal. The couplings  $f_{01}(\mathbf{k})$ ,  $f_{10}(\mathbf{k})$ ,  $f_{12}(\mathbf{k})$  and  $f_{21}(\mathbf{k})$  vanish since the spin orientation in the state  $|1\rangle$  differs from that in  $|0\rangle$  and  $|2\rangle$  (the effects of the spin-orbit coupling are discussed separately below). Moreover, it is assumed that there is no overlap of wave-functions between the states  $|0\rangle$  and  $|2\rangle$ , so that also  $f_{02}(\mathbf{k})$  and  $f_{20}(\mathbf{k})$  vanish.

An important point is that, since the electron resides normally in the large dot, at the initial moment the lattice is relaxed to the corresponding minimum (“dressing” of the electron in the coherent deformation field). This may be accounted for by defining the modes with respect to this shifted equilibrium, so that the ground state of the interacting system corresponds to the new phonon vacuum, i.e., by transforming to new phonon operators  $b_{\mathbf{k}}$  according to

$$b_{\mathbf{k}} = \beta_{\mathbf{k}} + \frac{f_{00}^*(\mathbf{k})}{\omega_{\mathbf{k}}}. \quad (24)$$

Upon transformation to these new modes the interaction reads

$$V = \sum_{n=2,3} |n\rangle\langle n| \sum_{\mathbf{k}} F_{nn}(\mathbf{k}) \left( b_{\mathbf{k}} + b_{-\mathbf{k}}^\dagger \right) + \left[ \sum_{n=0}^2 |n\rangle\langle 3| \sum_{\mathbf{k}} f_{n3}(\mathbf{k}) \left( b_{\mathbf{k}} + b_{-\mathbf{k}}^\dagger \right) + \text{H.c.} \right],$$

where  $F_{nn}(\mathbf{k}) = f_{nn}(\mathbf{k}) - f_{00}(\mathbf{k})$ . Moreover, the carrier Hamiltonian undergoes a renormalization which is, however, inessential for our discussion. In the rotating frame the above interaction Hamiltonian reads

$$V = \sum_{n=2,3} |\tilde{n}\rangle\langle \tilde{n}| \sum_{\mathbf{k}} F_{nn}(\mathbf{k}) \left( b_{\mathbf{k}} + b_{-\mathbf{k}}^\dagger \right) + \left[ \sum_{n=0}^2 |\tilde{n}\rangle\langle 3| \sum_{\mathbf{k}} F_{n3}(\mathbf{k}) \left( b_{\mathbf{k}} + b_{-\mathbf{k}}^\dagger \right) + \text{H.c.} \right]. \quad (25)$$

where  $F_{n3}(\mathbf{k}) = f_{n3}(\mathbf{k})e^{-i(\omega_n t - \delta_0)}$ . This Hamiltonian is of the form (2) with  $S_{nn'} = |n\rangle\langle n'|$  and  $R_{nn'} = \sum_{\mathbf{k}} F_{nn'}(\mathbf{k})(b_{\mathbf{k}} + b_{-\mathbf{k}})$ . The spectral densities [Eq. (10)] have the explicit form

$$R_{nn',mm'}(\omega) = \frac{1}{\hbar^2} \sum_{\mathbf{k}} F_{nn'}(\mathbf{k}) F_{m'm}^*(\mathbf{k}) \times [(n_{\mathbf{k}} + 1)\delta(\omega - \omega_{\mathbf{k}}) + n_{\mathbf{k}}\delta(\omega + \omega_{\mathbf{k}})], \quad (26)$$

where  $n_{\mathbf{k}}$  are phonon occupation numbers. Note that not all possible couplings appearing in the general form of Eq. (2) are present in our case. It is clear from Eq. (25) that the phonons influence the dynamics only when a transfer from the large dot to a spatially different carrier state (small dot or trion state) occurs.

The interaction potential given by Eq. (25) will be used in the calculation of phonon-induced decoherence according to the general theory of Sec. II. First, however, one has to describe the unperturbed evolution which is the second necessary ingredient of the calculation. This is done in the following section.

#### IV. THE STIRAP PROCEDURE FOR A SINGLE-QUBIT ROTATION

In this section we present the formal description<sup>21,22</sup> of the stimulated Raman adiabatic passage without external perturbation. Along with the results of the previous section this will allow us to use the general theory of Sec. II for the description of phonon-induced dephasing.

The system is modeled by the Hamiltonian given by Eq. (18). The envelopes of the first two pulses,  $\Omega_{0,1}$ , are chosen proportional to each other so that they may be written as

$$\Omega_0(t) = \Omega_{01}(t) \cos \chi, \quad \Omega_1(t) = \Omega_{01}(t) \sin \chi,$$

with a certain parameter  $\chi \in (0, \frac{\pi}{2})$  defining the fixed ratio of the pulse intensities. In terms of the new basis states

$$\begin{aligned} |B\rangle &= \cos \chi |\tilde{0}\rangle + e^{-i\tilde{\delta}_1} \sin \chi |\tilde{1}\rangle, \\ |D\rangle &= -\sin \chi |\tilde{0}\rangle + e^{-i\tilde{\delta}_1} \cos \chi |\tilde{1}\rangle, \end{aligned}$$

the Hamiltonian (18) now reads

$$H_C = \hbar \Delta |3\rangle\langle 3| + \frac{\hbar}{2} \Omega_{01}(t) (|B\rangle\langle 3| + |3\rangle\langle B|) + \frac{\hbar}{2} \Omega_2(t) (e^{-i\tilde{\delta}_2} |\tilde{2}\rangle\langle 3| + e^{i\tilde{\delta}_2} |3\rangle\langle \tilde{2}|). \quad (27)$$

Thus, the parameters  $\chi$  and  $\tilde{\delta}_1$  define two orthogonal states in the qubit space. The laser pulses affect only one of these states, the coupled (bright) state  $|B\rangle$ , while the other orthogonal combination,  $|D\rangle$ , remains unaffected.

At a fixed time  $t$ , the Hamiltonian (27) has the eigenstates

$$|a_0\rangle = \cos \theta |B\rangle - e^{-i\tilde{\delta}_2} \sin \theta |\tilde{2}\rangle \quad (28a)$$

$$|a_-\rangle = \cos \phi (e^{i\tilde{\delta}_2} \sin \theta |B\rangle + \cos \theta |\tilde{2}\rangle) - e^{i\tilde{\delta}_2} \sin \phi |3\rangle, \quad (28b)$$

$$|a_+\rangle = \sin \phi (\sin \theta |B\rangle + e^{-i\tilde{\delta}_2} \cos \theta |\tilde{2}\rangle) + \cos \phi |3\rangle, \quad (28c)$$

where

$$\tan \theta = \frac{\Omega_{01}}{\Omega_2}, \quad \sin \phi = \frac{1}{\sqrt{2}} \left( 1 - \frac{\Delta}{\sqrt{\Delta^2 + \Omega_{01}^2 + \Omega_2^2}} \right)^{1/2}.$$

The corresponding eigenvalues are  $\hbar \lambda_{0,\pm}$ , where

$$\lambda_0 = 0, \quad \lambda_{\pm} = \frac{\Delta \pm \sqrt{\Delta^2 + \Omega_{01}^2 + \Omega_2^2}}{2}. \quad (29)$$

The system evolution is realized by an adiabatic change of the pulse amplitudes (see Fig. 1; in this application, the detuning remains constant). Initially (at the time  $-t_0$ ), both pulses are switched off, hence  $\phi = 0$ , then  $\Omega_2$  is switched on first, hence also  $\theta = 0$ . Therefore,  $|a_0\rangle$  coincides with  $|B\rangle$  and  $|a_-\rangle$  with  $|\tilde{2}\rangle$ . During an adiabatic evolution of the parameters, the states move along the corresponding spectral branches. During the first passage,  $\tilde{\delta}_2 = 0$  and  $\theta$  is changed from 0 to  $\pi/2$ . At the end of this stage, when the pulses are switched off ( $\phi = 0$ ), the electron is in the state  $-\tilde{2}$ . The second passage takes  $\theta$  back from  $\pi/2$  to 0. Now, however,  $\tilde{\delta}_2 \neq 0$  so that the adiabatically followed system state is  $e^{i\tilde{\delta}_2} |a_0\rangle$  and the final state is  $e^{i\tilde{\delta}_2} |B\rangle$ . Note that the desired system evolution relies on the angle  $\theta$  determined by the ratio  $\Omega_{01}/\Omega_2$  (so called mixing angle), while the absolute value of these pulse amplitudes remains a free parameter that may be used for optimization against decoherence effects.

The evolution operator corresponding to this procedure may be written (in the basis  $|B\rangle, |\tilde{2}\rangle, |3\rangle$ )

$$U_C(t) = \begin{pmatrix} e^{i\tilde{\delta}_2} \cos \theta & e^{-i\Lambda_- + i\tilde{\delta}_2} \cos \phi \sin \theta & e^{-i\Lambda_+} \sin \phi \sin \theta \\ -\sin \theta & e^{-i\Lambda_-} \cos \phi \cos \theta & e^{-i(\tilde{\delta}_2 + \Lambda_+)} \sin \phi \cos \theta \\ 0 & -e^{-i\Lambda_- + i\tilde{\delta}_2} \sin \phi & e^{-i\Lambda_+} \cos \phi \end{pmatrix}, \quad (30)$$

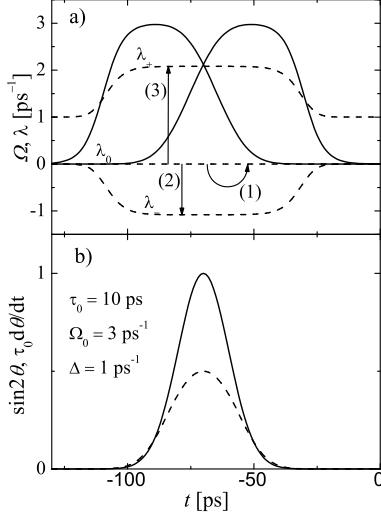


FIG. 1: (a) An example of pulse shapes (solid) and the resulting structure of the dresses levels (dashed). The arrows show the phonon-assisted transitions, as described in Sec. V: (1) the pure dephasing effect, (2,3) the transitions between the trapped states. (b) The evolution of the functions  $\dot{\theta}$  (dashed) and  $\sin 2\theta$  (solid) for the pulse sequence shown in (a).

where  $\theta, \phi, \lambda_{\pm}$  are slowly varying functions of time,  $\tilde{\delta}_2 = 0$  for  $t < 0$  and

$$\Lambda_{\pm}(t) = \int_0^t d\tau \lambda_{\pm}(\tau).$$

As shown in Ref. 21, the phase shift of the bright state resulting from the procedure described above is equivalent to the rotation in the qubit space  $|0\rangle, |1\rangle$  around the axis determined by  $\chi$  and by the relative phase  $\tilde{\delta}_1$  between  $\Omega_0$  and  $\Omega_1$ . The rotation angle is equal to the  $\tilde{\delta}_2$  phase of the second pulse sequence. The characteristic feature of the STIRAP is that no special form of the pulses is required. Thus, from the point of view of the unperturbed evolution, the detuning  $\Delta$  and the pulse envelopes  $\Omega_{0,2}$  are to a large extent arbitrary. This freedom may be used for minimizing the perturbing effects of the environment.

Ideally, the state  $|2\rangle$  is only occupied during gating, while the state  $|3\rangle$  is never occupied. This is true under the assumption that the evolution is perfectly adiabatic. However, any change of parameters can never be infinitely slow and the probability of a jump from  $|a_0\rangle$  to one of the two other states  $|a_{\pm}\rangle$  remains finite. In the lowest order, the corresponding probability amplitudes are<sup>34</sup>

$$c_{\pm}(t) = \int_{-t_0}^t d\tau \langle a_{\pm}(\tau) | \dot{\psi}(\tau) \rangle \exp \left[ -i \int_{\tau}^t \lambda_{\pm}(\tau') d\tau' \right],$$

where  $\psi(t)$  is the state evolving adiabatically from the initial one. Let us write the general initial state in the

form

$$|\psi_0\rangle = \cos \frac{\vartheta}{2} |B\rangle - e^{i\varphi} \sin \frac{\vartheta}{2} |D\rangle. \quad (31)$$

The qubit rotation<sup>21</sup> is performed by two well separated, mirror-symmetric pulse sequences differing only by a phase. Thus, using the explicit formulas (28a-c) one may write

$$c_{\pm}(t) = \cos \frac{\vartheta}{2} e^{-i\Lambda_{\pm}(t)} [\tilde{c}_{\pm} - \tilde{c}_{\pm}^*], \quad (32)$$

where

$$\tilde{c}_{\pm} = \int_{-\infty}^{\infty} d\tau \left[ \frac{\sin \phi(\tau)}{\cos \phi(\tau)} \right] \dot{\theta}(\tau) e^{i\Lambda_{\pm}(\tau)}, \quad (33)$$

with  $\sin \phi(\tau)$ ,  $\cos \phi(\tau)$  corresponding to ‘+’ and ‘-’, respectively, and the integral involves only one pulse sequence. If the evolution induced by the pulse sequence is symmetric with respect to a certain time  $t_1$  (the time around which the pulse sequence arrives) the amplitude (33) may be written in the form  $\tilde{c}_{\pm} = ie^{i\Lambda_{\pm}(t_1)} |\tilde{c}_{\pm}|$ .

In order to discuss the general properties of the nonadiabatic jump amplitudes, let us write the evolution of  $\theta$  in the form

$$\theta(t) = \tilde{\theta} \left( \frac{t - t_1}{\tau_0} \right), \quad (34)$$

where  $\tilde{\theta}$  is a function of unit width, so that  $\tau_0$  is the time scale of the evolution of  $\theta$ . (The total duration of the gate, including two pulse sequences, is roughly an order of magnitude longer). If the functions  $\phi(t)$  and  $\lambda_{\pm}(t)$  change slowly around  $t = t_1$ , then

$$|\tilde{c}_{\pm}| \approx \left[ \frac{\sin \phi(t_1)}{\cos \phi(t_1)} \right] g_0[\tau_0 \lambda_{\pm}(t_1)],$$

where

$$g_0(x) = \int du \tilde{\theta}'(u) e^{iux}$$

is a function of unit width, with a fixed value at  $x = 0$  and vanishing for  $x \gg 1$  (here prime denotes the derivative with respect to the argument  $u$ ). Hence, the nonadiabatic jump amplitudes (32) are small when

$$|\lambda_{\pm}| \gg 1/\tau_0, \quad (35)$$

which is the standard adiabaticity condition.

It is interesting to note that for symmetric pulses the final transition probabilities (32) vanish for  $\Lambda_{\pm}(t_1) = (n + 1/2)\pi$ . This fact is due to destructive interference of the jump amplitudes during the first and the second pulse sequence. Although it might be tempting to exploit this cancellation and perform a successful passage for times and laser beam parameters that do not satisfy the condition (35), such a procedure requires a detailed

knowledge of the excitonic dipole moments and a precise control over the laser beam properties. Moreover, the cancellation takes place only in the final state, while during the process the other states are occupied, which leads to the non-vanishing occupation of the  $X^-$  state and to decoherence, contrary to the original motivation of this qubit implementation. In order to avoid these effects, the envelopes of the transition probabilities should be used as the actual bound to the nonadiabatic-jump-related error.

## V. INTERACTION WITH THE PHONON BATH DURING THE STIRAP PROCESS IN A QD SYSTEM

In this section we apply the general theory from Section II to the qubit rotation performed via a STIRAP process, as described in Section IV, implemented in the double-QD system.

In the Hamiltonian (25), the only non-vanishing non-diagonal coupling is  $F_{n3}(\mathbf{k})$ . Let us note, however, that for this coupling one has, according to (12),

$$Y_{n3}(\omega) = \sum_{mm'} \int dt e^{i[(\omega - \omega_n)t + \delta_n]} U_{Cnm}^* U_{C3m'} |\tilde{m}\rangle \langle \tilde{m}'|,$$

where  $U_{Cnm}$  are the elements of the evolution operator (30), varying at most with frequencies  $\sim \lambda_{\pm}$ . It is therefore clear that this function is peaked around  $\omega \approx -\omega_n$ , i.e., at the optical frequencies which are many orders of magnitude higher than any phonon frequencies present in  $R_{nn',mm'}(\omega)$  [Eq. (10)]. Thus, inter-band non-diagonal phonon couplings do not contribute to (15). This is consistent with the rotating wave approximation and may also be understood by noting that the second Born approximation accounts for processes that may be represented as a series of emission and absorption processes involving arbitrarily many photons but only one phonon. Each photon process takes the system from the states 0, 1, 2 to 3 with the exchange of a large energy while a non-diagonal phonon process produces the same state change but with negligible energy exchange. Thus, energy can never be conserved in a process involving the inter-band phonon term.

Since the adiabatic evolution  $U_C$  does not transfer qubit states into  $|3\rangle$ ,  $U_C^\dagger|3\rangle$  remains orthogonal to  $|B\rangle$ . Hence,  $Y_{33}(\omega)$  does not contribute to (15) and we may write

$$\delta = \int d\omega \frac{R(\omega)}{\omega^2} S(\omega), \quad R(\omega) \equiv R_{22,22}(\omega), \quad (36)$$

with

$$S(\omega) = \omega^2 \sum_n |\langle \psi_0 | Y_{22}^\dagger(\omega) | \psi_n \rangle|^2 = \sum_n |s_n(\omega)|^2, \quad (37)$$

where the sum runs over a complete set of states  $|\psi_n\rangle$  orthogonal to  $|\psi_0\rangle$ .

For the initial state (31), using the explicit evolution operator (30), the contributions from the three states  $|\psi_n\rangle = \sin \frac{1}{2} \vartheta |B\rangle + e^{i\varphi} \cos \frac{1}{2} \vartheta |D\rangle, |2\rangle, |3\rangle$  are, respectively,

$$s_1(\omega) = -\frac{\omega}{2} \sin \vartheta \int_{-\infty}^{\infty} dt e^{-i\omega t} \sin^2 \theta(t), \quad (38)$$

$$s_{2,3}(\omega) = -\frac{\omega}{2} \cos \frac{\vartheta}{2} \int_{-\infty}^{\infty} dt e^{-i\omega t} \times \begin{bmatrix} \cos \phi(t) \\ \sin \phi(t) \end{bmatrix} \sin 2\theta(t) e^{-i\Lambda_{\mp}(t) - i\tilde{\delta}_2}. \quad (39)$$

These three contributions correspond to transitions indicated graphically in Fig. 1.

Following the argument that led to Eq. (32), these functions may be written in the form

$$|s_n(\omega)| = 2u_n(\vartheta) \text{Re}[\tilde{s}_i(\omega)],$$

where  $u_1 = \frac{1}{2} \sin \vartheta$ ,  $u_{2,3} = \cos(\vartheta/2)$ , and

$$\begin{aligned} \tilde{s}_1(\omega) &= i \int dt e^{-i\omega t} \sin 2\theta(t) \dot{\theta}(t) \\ &= i e^{-i\omega t_1} |\tilde{s}_1(\omega)|, \end{aligned} \quad (40a)$$

$$\begin{aligned} \tilde{s}_{2,3}(\omega) &= -\frac{\omega}{2} \int dt e^{-i[\omega t + \Lambda_{\mp}(t) - \tilde{\delta}_2]} \begin{bmatrix} \cos \phi(t) \\ \sin \phi(t) \end{bmatrix} \sin 2\theta(t) \\ &= e^{-i[\omega t_1 + \Lambda_{\mp}(t_1) + \tilde{\delta}_2/2]} |\tilde{s}_{2,3}(\omega)| \end{aligned} \quad (40b)$$

where the integrals are now over one pulse sequence and the final equalities hold for symmetric pulse sequences.

Using the representation (34) of the system evolution and denoting the Fourier transform of  $\tilde{\theta}' \sin 2\tilde{\theta}$  by  $g_1(x)$  we find  $|\tilde{s}_1(\omega)| = g_1(\omega\tau_0)$ . Since  $t_1 \gg \tau_0$  and  $|s_1(\omega)|^2$  is integrated with the slowly varying spectral density, the oscillating terms do not contribute and one may write

$$|s_1(\omega)|^2 \approx \frac{1}{2} \sin^2 \vartheta |g_1(\omega\tau_0)|^2.$$

Hence, the function,  $s_1(\omega)$  is centered at  $\omega = 0$  and broadened by a factor  $1/\tau_0$  due to the time-dependence. It is responsible for the pure dephasing effect.<sup>29</sup> The resulting error, according to (36), will grow with broadening of  $s_1(\omega)$ , i.e., with decreasing process duration. Hence, similarly to the fundamental condition (35), it always favors slow operation. However, it is independent of the trapped level splittings and reflects only the low-frequency properties of the spectral density (at a given temperature). For  $R(\omega) \approx R_0 \omega^n$ ,  $n \geq 3$  this pure dephasing error at the temperature  $T$  is

$$\delta^{(\text{pd})} \sim \begin{cases} R_0 \tau_0^{-(n-1)}, & k_B T \ll \hbar/\tau_0 \\ R_0 \frac{k_B T}{\hbar} \tau_0^{-(n-2)}, & k_B T \gg \hbar/\tau_0. \end{cases} \quad (41)$$

It should be noted that the crossover from the low to high temperature behavior is governed only by the pulse



duration (irrespective of the system parameters) and for durations of the order of 10 ps it takes place at  $T \sim 0.1$  K.

By a similar argument, the two other functions may be approximately written as

$$|s_{2,3}(\omega)|^2 \approx \frac{(\omega\tau_0)^2}{2} \cos^2 \frac{\vartheta}{2} \begin{bmatrix} \cos^2 \phi \\ \sin^2 \phi \end{bmatrix} g_2^2 [(\omega + \lambda_{\mp})\tau_0],$$

where  $g_2(x)$  is the Fourier transform of  $\sin 2\tilde{\theta}(u)$ . These functions have a similar  $1/\tau_0$  broadening but are also shifted to the spectral position  $\omega = -\lambda_{\pm}$ . They describe the error resulting from phonon-assisted transitions between the trapped states  $|a_{0,\pm}\rangle$  (see Appendix B for further support to this interpretation). In view of the condition (35), this shift must be larger than the broadening and for rough estimates the latter may be neglected (if the spectral density varies slowly on the scale of this broadening; the role of oscillations in the spectral density is discussed below). Hence, one may write  $\delta_{\mp}^{(\text{tr})} = \delta_{+}^{(\text{tr})} + \delta_{-}^{(\text{tr})}$ , where

$$\begin{aligned} \delta_{\mp}^{(\text{tr})} &= \int d\omega \frac{R(\omega)}{\omega^2} |s_{2,3}(\omega)|^2 \\ &\approx R(-\lambda_{\mp}) \int d\omega \left| \frac{s_{2,3}(\omega)}{\omega} \right|^2. \end{aligned} \quad (42)$$

The error is therefore proportional to

$$\delta_{\pm}^{\text{tr}} \sim R(\lambda_{\pm})\tau_0. \quad (43)$$

Thus, for a fixed spectrum of the trapped states this error grows linearly in time (in the leading order), which is a usual characteristics of real transition processes.

In order to maximize the fidelity of the coherent operation, one must find the trade-off between the errors caused by phonon-assisted transitions (43), which favors short process durations, and the other two restrictions, related to pure dephasing (41) and to the general adiabaticity condition (35) both increasing for fast evolution. As can be seen from the orders of magnitude of the spectral characteristics determining the error [Fig. 2 and Eq. (36)], in general, the fidelity may be strongly decreased. However, contrary to the simple excitonic qubit case<sup>29</sup>, the STIRAP procedure in a QD system provides two ways to avoid this limitations.

First, due to the super-ohmic properties of the phonon spectral density,  $R(\omega) \sim \omega^n$ ,  $n \geq 2$ , all error contributions may in principle be minimized by locating the trapped levels  $\lambda_{\pm}$  in the low-frequency sector and decreasing them while simultaneously increasing the gate duration  $\tau_0$ .

Second, the values of  $\lambda_{\pm}$  may be chosen sufficiently far beyond the cut-off frequency. The contribution from the phonon-induced transitions and nonadiabaticity effects may then be arbitrarily small and the error is limited by the pure dephasing effect, restricting the possible gate speed-up. However, one should keep in mind that in the

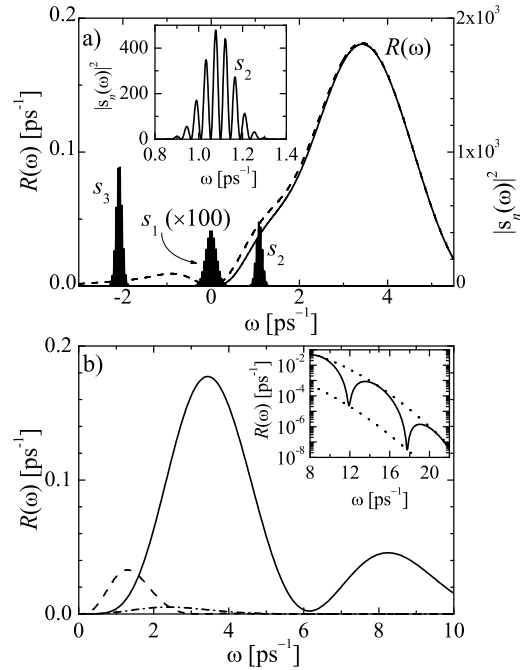


FIG. 2: (a) The functions  $|s_n(\omega)|^2$  describing the phonon-induced errors (for pulses as in Fig. 1) and the total spectral density of the phonon reservoir  $R(\omega)$  at  $T = 0$  (solid) and  $T = 5$  K (dashed) for the model InAs/GaAs system (Tab. I). The inset shows the exact shape of one of the spectral features. (b) The contributions to the spectral density at  $T=0$ : DP coupling to LA phonons (solid) and piezoelectric coupling to TA (dashed) and LA (dash-dotted) phonons. Inset: high-frequency behavior with the two bounds defined in Appendix A.

high frequency domain there may be additional reservoir excitations (including two-phonon processes) that are not accounted for in this model.

The error effects discussed here originate from the interaction between phonons and the orbital degrees of freedom used to operate the qubit. On the other hand, for a spin qubit one expects some contribution to the decoherence induced by the spin-orbit (SO) coupling. The electron confined in a quantum dot does not interact with other carriers so that, in contrast to higher-dimensional systems<sup>35,36,37</sup>, dephasing of the electron spin requires interaction with phonons<sup>38</sup> or nuclei<sup>39</sup>. In the Appendix C we analyze the former channel. We show there that the Markovian decay of spin states in our system is very slow and leads to negligible error over the times relevant for the qubit operations. On the other hand, non-Markovian SO-related effects induce the transitions between the same states as the direct phonon coupling but are many order of magnitude weaker due to very small SO-induced phonon coupling resulting from relatively large energy separation of orbital states. Thus, the SO-related effects do not affect the discussion presented here.

Electron effective mass	$m^*$	$0.067m_e$
Static dielectric constant	$\epsilon_s$	13.2
Piezoelectric constant	$d$	$0.16 \text{ C/m}^2$
Longitudinal sound speed	$c_l$	$5600 \text{ m/s}$
Transverse sound speed	$c_t$	$2800 \text{ m/s}$
Deformation potential for electrons	$\sigma$	$-8.0 \text{ eV}$
Density	$\rho_c$	$5360 \text{ kg/m}^3$
Landé factor	$g$	-0.44
Spin-orbit coupling constants:		
Rashba	$\alpha$	0
Dresselhaus	$\beta$	$1 \text{ nm/ps}$
Level separation	$\hbar\omega_0$	$46 \text{ meV}$
Electron wave-function widths:		
in-plane	$l_\perp$	$5.0 \text{ nm}$
z-direction	$l_z$	$1.5 \text{ nm}$
Dot separation	$D$	$6.0 \text{ nm}$

TABLE I: The GaAs material parameters and QD system parameters used in the calculations (after Refs. 40,41).

## VI. QUANTITATIVE RESULTS FOR A MODEL PULSE SEQUENCE

In this section we calculate the errors for a STIRAP operation on a single qubit performed with specific pulse shapes. In order to get quantitative estimates and to identify the key error-inducing mechanisms in various regimes of operation we use the material parameters and QD characteristics for an InAs/GaAs system which is frequently used as the “typical” system for the proposed qubit implementations. The system parameters are collected in the Table I.

It is known that the STIRAP procedure is rather insensitive to the exact pulse shape. In order to simplify the discussion, we choose the pulse sequence

$$\Omega_{01,2}(t) = \Omega_{\text{env}}(t) \left[ \frac{1 \mp \sqrt{1 - e^{-[(t \pm t_1)/\tau_0]^2}}}{2} \right]^{1/2},$$

which results in a very simple form for the time dependence of the mixing angle,

$$\sin 2\theta = e^{-\frac{1}{2}\left(\frac{t \pm t_1}{\tau_0}\right)^2}, \quad \dot{\theta} \approx \frac{1}{2\tau_0} e^{-\frac{1}{\pi}\left(\frac{t \pm t_1}{\tau_0}\right)^2}.$$

The envelope  $\Omega_{\text{env}}(t)$  may be any function approximately constant around  $t_1$ . For the numerical calculations we take

$$\Omega_{\text{env}}(t) = \Omega \frac{1 + \alpha}{1 + \alpha \cosh\left(\frac{t \pm t_1}{\tau_1}\right)},$$

with  $\alpha = 10^{-4}$ ,  $\tau_1 = 0.4\tau_0$  (Fig. 1 corresponds to this pulse choice).  $\Omega^2$  is proportional to the total power of the three pulses. The constant  $\Omega$ , along with  $\Delta$ , must be tuned for minimizing the decoherence effect.

For such a pulse sequence one finds explicitly from Eqs. (32,33)

$$\begin{aligned} |c_\pm|^2 &= 4\pi \cos^2 \frac{\vartheta}{2} \left[ \frac{\sin^2 \phi}{\cos^2 \phi} \right] \sin^2[\Lambda_\pm(t_1)] e^{-2(\lambda_\pm \tau_0)^2} \\ &\leq 4\pi \cos^2 \frac{\vartheta}{2} \left[ \frac{\sin^2 \phi}{\cos^2 \phi} \right] e^{-2(\lambda_\pm \tau_0)^2}, \end{aligned}$$

where the envelope of the oscillations has been taken as the safe bound to the error, in accordance with the discussion in Sec. IV. For the purpose of analytical estimates the values of  $\phi = \phi(t_1)$  and  $\lambda_\pm = \lambda_\pm(t_1)$  are assumed constant. The resulting error is equal to the sum of the two transition probabilities  $|c_\pm|^2$  and depends on the initial state (31), since  $c_\pm = c_\pm(\vartheta, \varphi)$ . The error averaged over the initial states is

$$\begin{aligned} \delta^{(\text{na})} &= \\ &= \frac{1}{4\pi} \int d\varphi \int d\vartheta \sin \vartheta (|c_+(\vartheta, \varphi)|^2 + |c_-(\vartheta, \varphi)|^2) \\ &= 2\pi \left[ \sin^2 \phi e^{-2(\lambda_- \tau_0)^2} + \cos^2 \phi e^{-2(\lambda_+ \tau_0)^2} \right]. \end{aligned} \quad (44)$$

The spectral functions  $s_i(\omega)$  relevant for the phonon-induced dephasing are

$$|s_1(\omega)|^2 = \frac{1}{2} \sin^2 \vartheta \frac{\pi^2}{2 + \pi} \sin^2(\omega t_1) e^{-\frac{\pi}{2+\pi}(\omega \tau_0)^2} \quad (45)$$

and

$$\begin{aligned} |s_{2,3}(\omega)|^2 &= 2\pi \cos^2 \frac{\vartheta}{2} (\omega \tau_0)^2 \cos^2[\omega t_1 + \Lambda_\mp(t_1)] \\ &\times \left[ \frac{\cos^2 \phi}{\sin^2 \phi} \right] e^{-(\omega + \lambda_\mp)^2 \tau_0^2}. \end{aligned} \quad (46)$$

The total error is calculated as the sum of the non-adiabatic jump probability (44) and the phonon-induced contributions given by (36,37) with the spectral functions (45) and (46). The phonon spectral density corresponding to our model double-dot InAs/GaAs system is derived and discussed in the Appendix A and plotted in Fig. 2.

The resulting error, averaged over  $(\vartheta, \varphi)$  as in Eq. (44), as a function of the pulse intensity parameter  $\Omega$  and detuning  $\Delta$  for a fixed process duration  $\tau_0$  is shown in Fig. 3. The nontrivial interplay of the three error contributions discussed above together with the oscillating high-frequency tail of the phonon density of states  $R(\omega)$  (see inset in Fig. 2b) lead to an intricate parameter dependence of the total error. There are clearly several parameter combinations for which the error becomes small. With the help of the formulas (29) one finds that the area (0a) corresponds to  $\lambda_-$  in the low-frequency region, while in (0b)  $\lambda_+$  is small and  $\lambda_-$  shifted beyond the phonon cut-off. The valleys (1), (2) ... correspond to  $\lambda_-$  positioned at one of the minima in the high-frequency tail of  $R(\omega)$  and  $\lambda_+$  shifted beyond the thermal cut-off for phonon-absorption processes, i.e.  $\hbar\lambda_+ \gtrsim k_B T$ . For  $T = 0$  the

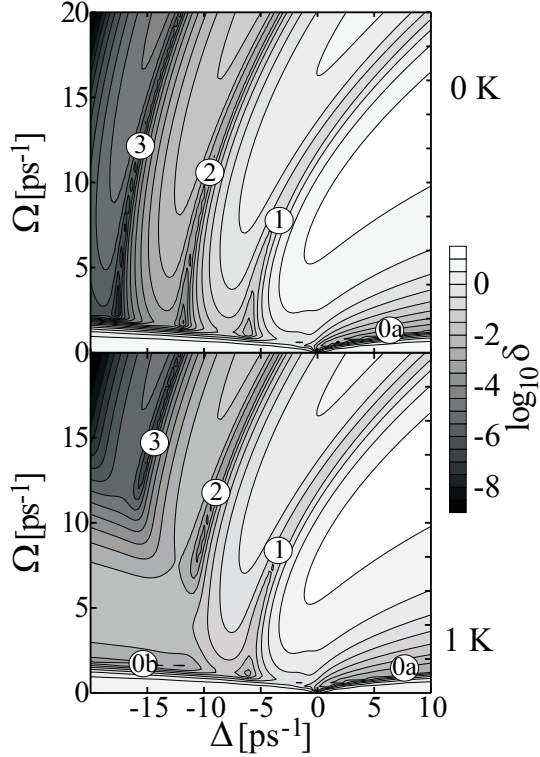


FIG. 3: The dependence of  $\log_{10} \delta$  on the pulse parameters  $\Delta$  and  $\Omega$  at  $T = 0$  and  $T = 1$  K for  $\tau_0 = 50$  ps. Numbers refer to the parameter regimes discussed in the text.

absorption processes are not allowed at all and these areas are not separated from the (0b) region.

The detailed analysis of the error value along the (0a) valley at various temperatures (Fig. 4a) shows that at  $T \neq 0$  the dependence is not monotonous. The absolute minimum always corresponds to very low  $\Omega$  and  $\Delta$ , for which both trapped states  $\lambda_{\pm}$  lie in the low frequency region. At high frequencies, the error values reach a plateau after passing (at  $T > 0$ ) through a second, very shallow minimum (due to the subtle interplay of the error contributions weighted by the parameter-dependent  $\sin \phi$  and  $\cos \phi$  factors). In between, there is either a monotonous increase (at  $T \rightarrow 0$ ) or a transition through a local maximum, as the  $\lambda_+$  state crosses the frequency sector with high spectral density for phonon absorption (cf. Fig 2). Fig. 4b shows the interplay between different error contributions when the Rabi frequency  $\Omega$  is changed for a fixed detuning  $\Delta$ . In this range of parameters, for the specific system under study, the pure dephasing contribution turns out to be small compared to the errors related to real phonon-induced transitions and to nonadiabatic jumps which create a trade-off situation with one or two well-defined parameter sets corresponding to the minimal errors.

The above results show that for a fixed pulse duration  $\tau_0$  the error values are bounded from below, precluding

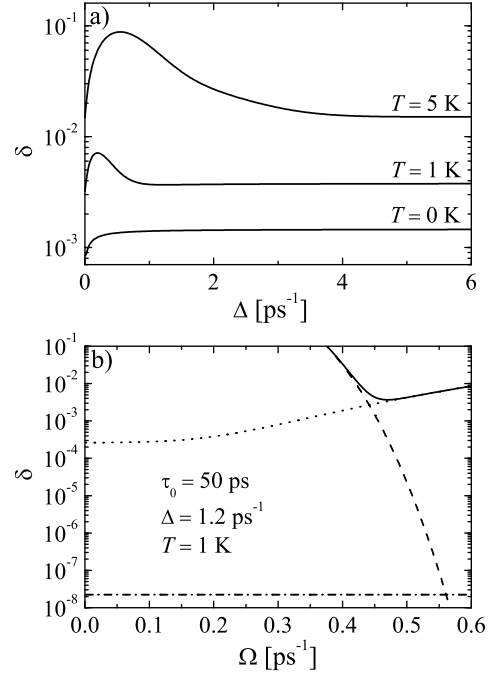


FIG. 4: (a) The dependence of the error for growing detuning with  $\lambda_- = \text{const}$ , along the (0a) minimum in Fig. 3. (b) The total error (solid) and the individual contributions: nonadiabatic jumps (dashed), phonon-assisted real transitions (dotted) and pure dephasing (dash-dotted) for a section of the parameter space.

a perfect operation for any parameter values. However, due to the super-ohmic behavior of all the contributions to the phonon spectral density (at low frequencies), the total error is decreased when the process time grows and the trapped level splittings decrease. The minimum error achievable for different process durations at various temperatures is plotted in Fig. 5a,b and the corresponding laser beam parameters are shown in Fig. 5c,d. Both the values at the global minimum (Fig. 5a,c) and at the shallow local minimum (Fig. 5b,d) are shown. In order to allow for any subtle interplay of parameters, for each  $\tau_0$  the full minimization with respect to both  $\Delta$  and  $\Omega$  was performed. As expected, the error decreases for longer pulse durations, but the decrease is only polynomial ( $\delta \sim 1/\tau_0$  at higher temperatures and  $\tau_0 \gtrsim 10$  ps). Therefore, rather long pulse durations are necessary to reduce the error considerably. Moreover, the optimization is obtained for rather unusually small parameter values (Fig. 5b) and is very sensitive to their precision. Still another restriction is that in this low-frequency regime the optimum is searched against the nonadiabatic jump error and is reached for  $\tau_0 \lambda_{\pm} \gtrsim 1$ . As soon as  $\tau_0$  becomes comparable to the trion radiative lifetime ( $\sim 1$  ns), the optimal value of  $\lambda_{\pm}$  falls within the broadening of the  $|3\rangle$

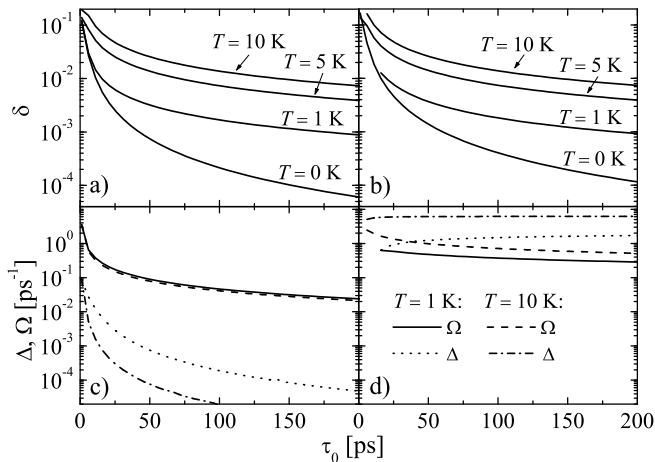


FIG. 5: (a,b) The minimal achievable error as a function of the process duration corresponding to the optimal pulse parameters with both  $\lambda_{\pm}$  in the low-frequency area (a) and with  $\lambda_{+}$  in the high frequency area (b) (for  $T = 0$  the plateau value for  $\Delta \rightarrow \infty$  is shown). (c,d) The optimal pulse parameters (detuning and Rabi frequency) realizing the minimal error for these two configurations. The legend in (d) applies to both (c,d).

state, disabling the adiabatic passage.

The parameter dependence of the error in the (0b) area is in a way analogous. Here, however, it is  $|\lambda_{-}|$  that must be shifted far beyond the positive frequency cut-off. Even at zero temperature, the positive-frequency part of the spectral density extends to relatively high frequencies (with oscillations manifesting themselves as local minima in Fig. 3b). Therefore, this parameter regime is always less favorable than the previous one.

In view of the limited possibility of fidelity optimization in the low-frequency region for reasonable process durations, it is interesting to study the high-frequency parameter range. In contrast to the previous case, the values of  $\Omega$  and  $\Delta$  may now seem unusually high, but the results of Fig. 3 show that by increasing the splitting between the trapped state energies the error may in principle be reduced to arbitrarily low values.

The Figure 6 shows the error along the (1) and (2) areas (Fig. 3) for fixed pulse duration at various temperatures, as well as the contributions to the error in one case. The trapped states are now split by several meV, so that the nonadiabatic error is negligible (except for sub-picosecond pulses). However, the speeding-up of the dynamics is limited by the pure-dephasing contribution. On the other hand, extending the pulse duration is unfavorable due to the phonon-assisted transitions. The interplay of these two contributions for a given pulse duration, temperature, and  $\lambda_{-}$  yields a series of minima, corresponding to  $\lambda_{+}$  traveling across the oscillations of  $R(\omega)$ , as shown in Fig. 6. Note that at low temperatures only one minimum exists, belonging actually to the (0b) parameter area, but at higher temperatures the absolute

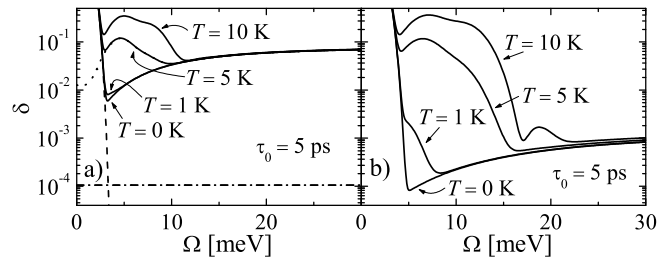


FIG. 6: The error as a function of  $\Omega$  for  $\lambda_{-} = \text{const}$ , along the 1 (a) and 2 (b) areas in Fig. 3. In (a) the individual contributions to the error at  $T = 5$  K are also shown: nonadiabatic jumps (dashed), phonon-assisted real transitions (dotted) and pure dephasing (dash-dotted).

minimum shifts to the high-frequency region.

The minimum value reached depends on the pulse duration, with a certain optimal trade-off which depends, however, on the chosen value of  $\lambda_{-}$  and decreases substantially for subsequent minima of the spectral density. The resulting minimum value, obtained by numerical minimization with respect to  $\Omega$  and  $\Delta$  for a range of pulse durations, is shown in Fig. 7a,b. The individual contributions shown in Fig. 7a show that pure dephasing indeed limits the fidelity for short pulses but in the optimal duration range the non-monotonous  $\tau_0$ -dependence of the error is determined exclusively by the phonon-assisted transition contribution. This astonishing effect is in fact due to the relatively narrow minimum of  $R(\omega)$  in which  $|\lambda_{-}|$  is placed. For short pulses,  $s_3(\omega)$  becomes broad (pure dephasing broadening of the  $\lambda_{-}$  level), increasing the overlap with  $R(\omega)$ . For large  $\tau_0$ , the linear increase of  $\delta$  due to long process duration becomes dominating, leading to a minimum at a certain point.

## VII. CONCLUSIONS

We have studied the fidelity of the coherent operation on a QD spin qubit rotated by a stimulated Raman adiabatic passage to a neighboring dot and back. We have shown that, in addition to the usual limitation of the speed of an adiabatic process, the presence of the phonon reservoir imposes two further restrictions: The transfer must be slow in order to minimize the pure dephasing effect but it should not take too long in order to avoid transitions between the trapped carrier-light states. The general formalism was applied to an InAs/GaAs self-assembled system of typical size. It turns out that for most values of pulse parameters (pulse intensities and detuning) in meV range the error is high enough to totally prevent the coherent operation. However, there are also narrow parameter areas where the fidelity is considerably higher.

The super-ohmic characteristics of the spectral density

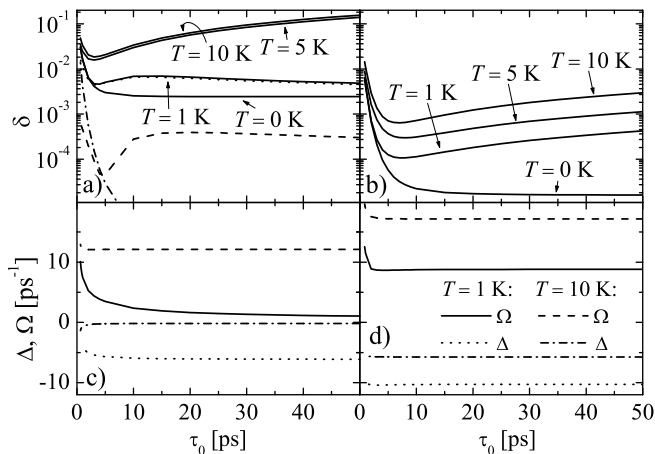


FIG. 7: (a,b) The minimal achievable error as a function of the process duration corresponding to the optimal pulse parameters with both  $\lambda_{\pm}$  in the high-frequency parameter areas 1 (a) and 2 (b) and the optimal pulse parameters (detuning and Rabi frequency) realizing the minimal error for these two configurations (c,d). In (a) the contributions to the error at  $T = 1$  K are shown: nonadiabatic jumps (dashed), phonon-assisted real transitions (dotted) and pure dephasing (dash-dotted).

associated with the phonon reservoir admits minimization of the total error by increasing the duration of the process while simultaneously decreasing the trapped level energies. However, the pulse durations necessary for a considerable reduction of the error in this low-frequency regime are of order of hundreds of picoseconds which leads to nanosecond overall gate durations (full sequence of two pairs of pulses). Moreover, the resulting trapped state energies become extremely small, approaching the typical lifetime broadening of the trion state used for the Raman coupling.

It is found that the qubit operation may be performed with much higher fidelity if the trapped states are pushed beyond the cut-off of the effectively coupled phonon modes. An additional advantage comes from the oscillatory structure of the phonon spectral density for a double-dot system. In this way the error at  $T = 0$  may be reduced to the value of  $\sim 10^{-3}$  and well below  $10^{-4}$  for the trapped state energy splitting of 4 meV and 8 meV, respectively (for the system geometry assumed here). The latter values lie in the spectral region where the acoustic phonon effects dominate the decoherence, well below any spectral features (LO phonons, higher exciton states) not included in the discussion. It is remarkable that such low error values are achieved with pulse durations of the order of 10 ps which, compared to the long electron spin decoherence time, even up to tens of milliseconds<sup>42</sup>, opens a broad time window for a large number of gating operations.

We have analyzed also the errors related to the spin-orbit coupling. It turns out that these effects are negli-

gible in the present implementation.

These optimistic conclusions are somewhat limited by the strong temperature dependence of phonon occupations, especially in the low-frequency regime, leading to a fast increase of the error at non-zero temperatures. Indeed, in some cases the minimal error may grow even by an order of magnitude as soon as the temperature reaches 1 K.

The strong dependence of the phonon-related error on the material parameters and system geometry opens some possibility of system engineering and optimization. For example, the high-frequency asymptotics of the phonon spectral density is governed by the QD height: higher dots assure a faster decay. On the other hand, in the low-frequency sector the phonon spectral density scales with the square of the inter-dot distance, favoring rather flat structures. Also increasing the lateral size reduces the phonon coupling but, at the same time, lowers the excited states restricting the high-frequency range of operation. This shows that finding the optimum may be nontrivial and may depend on the frequency sector chosen for the qubit operation. It should be noted that the high-frequency spectral density is dominated by the deformation potential coupling which is present in any semiconductor system but in the low-frequency domain the piezoelectric effects dominate. This might suggest using non-piezoelectric materials.

Let us note also that the single-qubit error calculated in this paper gives also an estimate of the two-qubit operation if the latter is performed using dipole coupling between the auxiliary states in the STIRAP scheme.<sup>18</sup>

## Acknowledgments

This work was supported by the Polish Ministry of Scientific Research and Information Technology under the (solicited) Grant No. PBZ-MIN-008/P03/2003 and by the Polish KBN under Grant No. PB 2 P03B 08525. P.M. is grateful to the Humboldt Foundation for support.

## APPENDIX A: PHONON COUPLINGS AND SPECTRAL DENSITIES

In this Appendix we derive the spectral density of the phonon reservoir  $R_{22}(\omega)$  and study its properties for low and high frequencies.

The phonon coupling constants  $F_{22}(\mathbf{k}) = f_{22}(\mathbf{k}) - f_{00}(\mathbf{k})$  have the same structure as the original constants [Eq. (20a,b)] with the form factor replaced by  $\mathcal{F}(\mathbf{k}) = \mathcal{F}_{22}(\mathbf{k}) - \mathcal{F}_{00}(\mathbf{k})$ . Let  $\mathcal{F}_{L,S}(\mathbf{k})$  denote the form factors, calculated according to Eq. (23), for the ground-state electronic wave-function in the large (L) and small (S) dot. Assuming that the dots are stacked along the  $z$  axis at the distance  $D$ , one has

$$\mathcal{F}(\mathbf{k}) = e^{i\frac{Dk_z}{2}} \mathcal{F}_S(\mathbf{k}) - e^{-i\frac{Dk_z}{2}} \mathcal{F}_L(\mathbf{k}).$$

The long-wavelength properties of the coupling constants do not depend on the wave-function geometry. Indeed,  $\mathcal{F}_{S,L}(\mathbf{k}) = 1 + O(k^2)$  and  $\mathcal{F}(\mathbf{k}) = iDk_z + O(k^3)$ .

The coupling constants for arbitrary  $\mathbf{k}$  depend obviously on the specific form of the wave-functions. For simplicity, we assume Gaussian wave-functions,

$$\Psi_{L,S}(\mathbf{r}) = N \exp \left[ -\frac{1}{2} \left( \frac{\mathbf{r}_\perp}{l_{\perp L,S}} \right)^2 - \frac{1}{2} \left( \frac{z}{l_{z L,S}} \right)^2 \right].$$

Then

$$\mathcal{F}_{S,L}(\mathbf{k}) = e^{-\left(\frac{k_\perp l_{\perp L,S}}{2}\right)^2} e^{-\left(\frac{k_z l_{z L,S}}{2}\right)^2}. \quad (\text{A1})$$

Allowing for a small difference between the dot sizes we write  $l_{\perp L,S}^2 = l_\perp^2 \pm \frac{1}{2}\Delta(l_\perp^2)$ ,  $l_{z L,S}^2 = l_z^2 \pm \frac{1}{2}\Delta(l_z^2)$ , so that

$$\begin{aligned} \mathcal{F}(\mathbf{k}) &\approx \\ &e^{-\left(\frac{k_\perp l_\perp}{2}\right)^2} e^{-\left(\frac{k_z l_z}{2}\right)^2} \\ &\times \left[ 2i \sin \frac{Dk_z}{2} + \frac{k_\perp^2 \Delta(l_\perp^2) + k_z^2 \Delta(l_z^2)}{4} \cos \frac{Dk_z}{2} \right]. \end{aligned}$$

Hence, the size difference brings only a small correction and will be neglected.

Assuming isotropic phonon dispersions, the spectral density  $R(\omega) = R_{22,22}(\omega)$  [Eq. (10)] may be written as

$$\begin{aligned} R(\omega) &= \frac{V}{(2\pi)^3} \sum_s \int dk k^2 \\ &\times [(n_k + 1)\delta(\omega - \omega_k) + n_k \delta(\omega + \omega_k)] \\ &\times \frac{1}{\hbar^2} \int \cos \theta d\theta \int d\varphi |F_{22}^{(s)}(\mathbf{k})|^2. \end{aligned}$$

The LA phonons are coupled both via piezoelectric and deformation potential interaction. However, due to different inversion symmetry the mixed terms vanish upon angle integration and the two terms contribute independently.

The deformation potential term is

$$R^{(\text{DP})}(\omega) = R_0^{(\text{DP})} \omega^5 [n_B(\omega) + 1] f^{(\text{DP})}(\omega),$$

where

$$R_0^{(\text{DP})} = \frac{1}{3(2\pi)^2} \frac{D^2 \sigma_e^2}{\hbar \rho_c c_1^7}$$

and the function  $f^{(\text{DP})}(\omega)$  is defined as

$$\begin{aligned} f^{(\text{DP})}(\omega) &= \frac{3}{2} \int_{-\pi/2}^{\pi/2} d\theta \cos \theta \frac{4 \sin^2 \left( \frac{D\omega}{2c_1} \sin \theta \right)}{\left( \frac{D\omega}{2c_1} \right)^2} \\ &\times \exp \left[ -\frac{1}{2} \left( \frac{\omega l_\perp}{c_1} \right)^2 \left( \cos^2 \theta + \frac{l_z^2}{l_\perp^2} \sin^2 \theta \right) \right], \end{aligned} \quad (\text{A2})$$

so that  $f^{(\text{DP})}(\omega) \rightarrow 1$  as  $\omega \rightarrow 0$ .

For the piezoelectric contributions we choose the phonon polarizations

$$\begin{aligned} \hat{e}_{1,\mathbf{k}} &\equiv \hat{\mathbf{k}} = (\cos \theta \cos \phi, \cos \theta \sin \phi, \sin \theta), \\ \hat{e}_{t1,\mathbf{k}} &= (-\sin \phi, \cos \phi, 0), \\ \hat{e}_{t2,\mathbf{k}} &= (\sin \theta \cos \phi, \sin \theta \sin \phi, -\cos \theta); \end{aligned}$$

then the functions  $M_s$  [Eq. (21)] are

$$\begin{aligned} M_1 &= \frac{3}{2} \sin 2\theta \cos \theta \sin 2\phi, \\ M_{t1} &= \sin 2\theta \cos 2\phi, \\ M_{t2} &= (3 \sin^2 \theta - 1) \cos \theta \sin 2\phi. \end{aligned}$$

The corresponding terms in the spectral density are

$$R^{(P)}(\omega) = \sum_s R_0^{(P,s)} \omega^3 [n_B(\omega) + 1] f^{(P,s)}(\omega), \quad (\text{A3})$$

where

$$R_0^{(P,s)} = \frac{1}{2\hbar \rho_c (2\pi)^3 c_s^5} \mu_s \left( \frac{edD}{\epsilon_0 \epsilon_s} \right)^2,$$

$$\begin{aligned} f^{(P,s)}(\omega) &= \frac{1}{\mu_s} \int_{-\pi/2}^{\pi/2} d\theta \cos \theta M_s^2(\theta) \frac{4 \sin^2 \left( \frac{D\omega}{2c_1} \sin \theta \right)}{\left( \frac{D\omega}{2c_1} \right)^2} \\ &\times e^{-\frac{1}{2} \left( \frac{\omega l_\perp}{c_1} \right)^2 \left[ \cos^2 \theta + \frac{l_z^2}{l_\perp^2} \sin^2 \theta \right]}, \end{aligned}$$

$f^{(P,s)}(\omega) \rightarrow 1$  as  $\omega \rightarrow 0$ , and

$$M_s^2(\theta) = \int d\varphi M_s^2(\theta, \varphi), \quad \mu_s = \int d\theta \cos \theta \sin^2 \theta M_s^2(\theta).$$

The specific values are  $\mu_1 = \mu_{t1} = 16\pi/35$ ,  $\mu_{t2} = 16\pi/105$ . Thus, the low-frequency behavior of the individual contributions to the spectral density is  $\sim \omega^3$  and  $\sim \omega^5$  for the piezoelectric and deformation potential coupling, respectively.

The behavior in the high frequency limit is determined by the coupling to phonons with wave vectors in the strongest confinement direction, i.e. along the  $z$  axis. The piezoelectric coupling in this direction is suppressed by the geometrical factors  $M_s$  and the corresponding contributions to the spectral function decrease rapidly. Moreover, the frequencies of TA phonons are relatively low and the piezoelectric coupling to LA phonons is much weaker. The frequencies of LA phonons reach much higher values, e.g. over 20 meV for GaAs, and their dispersion remains approximately isotropic and linear up to several meV.<sup>41</sup> Expanding the integral into an asymptotic series one finds an upper estimate for (A2),

$$f^{(\text{DP})}(\omega) \lesssim \frac{12c_1^4}{D^2(l_\perp^2 - l_z^2)} \frac{1}{\omega^4} e^{-\frac{1}{2} \left( \frac{l_z \omega}{c_1} \right)^2}.$$

In vicinity of the points  $\omega_n = 4n\pi c_1/D$ , the following lower bound approximately holds

$$f^{(\text{DP})}(\omega) \gtrsim \frac{3c_1^6}{(l_\perp^2 - l_z^2)^3} \frac{1}{\omega^6} e^{-\frac{1}{2}\left(\frac{l_z \omega}{c_1}\right)^2}, \quad (\text{A4})$$

(see Fig. 2b) The oscillatory behavior of the spectral density for large frequencies follows from the fact that the predominant contribution in this sector comes from phonons along the strongest confinement direction, leading to a pronounced destructive interference of interaction amplitudes in the double-dot structure aligned along this direction.

## APPENDIX B: TRANSITIONS BETWEEN THE TRAPPED STATES: FERMI GOLDEN RULE

In this Appendix we show that the error  $\delta_{\mp}^{(\text{tr})}$  [Eq. (42)] may be interpreted, in terms of the Fermi Golden Rule (FGR), as resulting from transitions between the trapped states of the confined electron in the external driving field [transitions (2) and (3) in Fig. 1].

Inserting the definition (40b) into the Eq. (42) and performing the frequency integration (for  $\lambda_{\pm}, \phi \approx \text{const}$ ) we get

$$\delta_{\mp}^{(\text{tr})} \approx \cos^2 \frac{\vartheta}{2} \frac{\pi}{2} R(-\lambda_{\mp}) \left[ \frac{\cos^2 \phi}{\sin^2 \phi} \right] \int dt \sin^2 2\theta(t). \quad (\text{B1})$$

Let us now consider the probability of phonon absorption or emission leading to a transition from the state  $|a_0\rangle$  to  $|a_{\pm}\rangle$ . The duration of a single absorption or emission process is of the order of the inverse phonon frequency (i.e. trapped level spacing). Hence, in view of the adiabaticity condition (35) this process is fast compared to the characteristic time scale of the system evolution. Therefore, it is reasonable to calculate the FGR probability for absorption or emission at fixed values of system parameters and include the time-dependence related to the STIRAP passage only at the level of the rate equations. Assuming the initial state (31), taking the matrix element of the phonon coupling Hamiltonian (25) between the trapped states (28a-c) and applying the FGR in the standard form one finds for the transition probability

$$\begin{aligned} w_{\mp}(t) &= \frac{2\pi}{\hbar} \frac{1}{4} \cos^2 \frac{\vartheta}{2} \left[ \frac{\cos^2 \phi}{\sin^2 \phi} \right] \sin^2 2\theta(t) \sum_{\mathbf{k}} |F(\mathbf{k})|^2 \\ &\quad \times [\delta(\hbar\lambda_{\mp} - \hbar\omega_{\mathbf{k}})n_{\mathbf{k}} + \delta(\hbar\lambda_{\mp} + \hbar\omega_{\mathbf{k}})(n_{\mathbf{k}} + 1)] \\ &= \frac{\pi}{2} \cos^2 \frac{\vartheta}{2} \left[ \frac{\cos^2 \phi}{\sin^2 \phi} \right] \sin^2 2\theta(t) R(-\lambda_{\mp}). \end{aligned}$$

Solving the rate equation for the jump probability with the above time-dependent rate  $w(t)$  we find the error probability for the whole process duration

$$\delta_{\mp}^{(\text{tr})} = 1 - \exp \left[ - \int_{-\infty}^{\infty} w_{\mp}(t) dt \right]. \quad (\text{B2})$$

For small error values this reduces to (B1). However, it gives also an estimate for the error beyond the applicability of the perturbative treatment.

## APPENDIX C: SPIN-FLIP EFFECTS DUE TO SPIN-ORBIT COUPLING

In the present Appendix, we discuss the additional error due to the presence of spin-orbit coupling for the electron. We will show that each of the spin-conserving dephasing channels discussed in the main body of the paper is accompanied by a spin-flip channel which is, however, several orders of magnitude weaker in a self-assembled system. There is, moreover, an additional error related to a spin-flip transition in the small dot but it is also extremely small.

We start the quantitative analysis by adding the spin-orbit coupling to the qubit Hamiltonian in Eq. (16),

$$H_C = H_d + H_Z + H_{\text{SO}} + H_L(t).$$

Here  $H_d = p^2/(2m^*) + U(\mathbf{r})$ , where  $m^*$  is the electron effective mass and  $U(\mathbf{r})$  is the confinement potential;  $H_Z = (1/2)g\mu_B B\sigma_y$  is the Zeeman energy ( $g$  is the effective Landé factor,  $\mu_B$  is the Bohr magneton and  $\sigma_y$  is the Pauli matrix; the magnetic field is oriented along  $y$ ),  $H_L(t)$  describes the coupling to the control laser field and  $H_{\text{SO}} = \beta(-p_x\sigma_x + p_y\sigma_y) + \alpha(p_x\sigma_y - p_y\sigma_x)$  is the spin-orbit term composed of the Rashba and Dresselhaus coupling with the constants  $\alpha$  and  $\beta$ , respectively.

Following Ref. 38, we look for the unitary transformation  $e^S$  that eliminates the spin-orbit coupling from the stationary Hamiltonian  $H_1 = H_d + H_Z + H_{\text{SO}}$ . To the leading order in the SO coupling one has

$$e^S H_1 e^{-S} = H_d + H_Z + H_{\text{SO}} + [S, H_d + H_Z].$$

For the harmonic confinement  $U(\mathbf{r}) = (1/2)m^*\omega_0^2(x^2 + y^2) + (1/2)m^*\omega_z^2 z^2$ ,  $\omega_z \gg \omega_0$ , the SO coupling is perturbatively eliminated with the choice

$$S = i \frac{g\mu_B B}{(\hbar\omega)^2} (\beta p_x - \alpha p_y) + \dots,$$

where we omitted an irrelevant position-dependent part.

Upon the canonical transformation, the electron-phonon Hamiltonian (19) becomes, in the leading order in the SO coupling,  $\tilde{V} = V + V_{\sigma}$ , where the additional term is

$$\begin{aligned} V_{\sigma} &= [S, V] \\ &= i \frac{g\mu_B B}{(\hbar\omega)^2} \sum_{\mathbf{k}} \hbar(\beta k_x - \alpha k_y) v_{\mathbf{k}} e^{i\mathbf{k}\cdot\mathbf{r}} (\beta_{\mathbf{k}} + \beta_{-\mathbf{k}}^{\dagger}) \sigma_z, \end{aligned}$$

where  $v_{\mathbf{k}}$  are defined by Eqs. (20a,b). Within the reduced subspace spanned by the relevant states, this operator has non-vanishing elements only between those states

that have overlapping wave functions and opposite  $\sigma_y$  spins. Thus, one has

$$V_\sigma = \sum_{\mathbf{k}} \left[ F_\sigma^{(S)}(\mathbf{k}) (|0\rangle\langle 1| e^{-iE_Z t/\hbar} + \text{H.c.}) + F_\sigma^{(L)}(\mathbf{k}) (|2\rangle\langle 2'| e^{-iE_Z t/\hbar} + \text{H.c.}) \right] (\beta_{\mathbf{k}} + \beta_{-\mathbf{k}}^\dagger),$$

where  $E_Z = g\mu_B B$  is the Zeeman energy splitting,  $|2'\rangle$  is the state in the ‘‘small’’ dot with flipped spin and

$$\begin{aligned} F_\sigma^{(S,L)}(\mathbf{k}) &= F_\sigma^{(S,L)*}(-\mathbf{k}) \\ &= i \frac{g\mu_B B}{(\hbar\omega)^2} \hbar (\beta_{k_x} - \alpha k_y) v_{\mathbf{k}} \mathcal{F}_{S,L}(\mathbf{k}) e^{\pm i \frac{k_z D}{2}}, \end{aligned} \quad (\text{C1})$$

with the form factors given by Eq. (A1).

Upon the phonon equilibrium shift given by Eq. (24), the above interaction Hamiltonian produces a small spin-dependent renormalization of the qubit Hamiltonian. More importantly, the canonical transformation implicitly performs a transition to the eigenstates of the full Hamiltonian including the SO term. These states may couple to the control field in a different manner than the original states, which is reflected in the present formalism by the correction terms resulting from the transformation  $\tilde{H}_L(t) = e^S H_L(t) e^{-S} = H_L(t) + H_L^{(1)}(t) + \dots$ . The feasibility of the STIRAP process in the presence of such spin-dependent terms is a separate problem, far beyond the scope of the present paper. Here we assume that the control field can be appropriately modified so that the new states may be evolved according to the same STIRAP transfer as the original ones. The weakness of the spin-dependent phonon effects, as discussed below, suggests that also these SO corrections might be of minor importance.

The SO contribution to the error may be written, in analogy to Eqs. (15,36), as

$$\delta_\sigma = \int d\omega R_\sigma(\omega) S_\sigma(\omega), \quad (\text{C2})$$

where

$$S_\sigma(\omega) = \omega^2 \sum_n |\langle \psi_n | Y_\sigma(\omega) | \psi_0 \rangle|^2, \quad (\text{C3})$$

with

$$\begin{aligned} Y_\sigma(\omega) &= \int_{-t_0}^{t_0} dt e^{i\omega t} U_C^\dagger(t) \\ &\times (|0\rangle\langle 1| e^{-iE_Z t/\hbar} + |2\rangle\langle 2'| e^{-iE_Z t/\hbar} + \text{H.c.}) U_C(t). \end{aligned}$$

The summation in Eq. (C3) now involves all the states  $|\psi_n\rangle$  orthogonal to  $|\psi_0\rangle$ , including  $|2'\rangle$ .

Similarly as in the Appendix A, we find the low-frequency expressions for the spectral densities [Eq. (10)] corresponding to the SO coupling (C1) via the two different coupling channels

$$R_\sigma^{(\text{DP})}(\omega) = R_{\sigma 0}^{(\text{DP})} \omega^5 [n_B(\omega) + 1], \quad (\text{C4})$$

where

$$R_{\sigma 0}^{(\text{DP})} = \frac{1}{12\pi^2} \frac{(g\mu_B B)^2}{(\hbar\omega_0)^4} \frac{\hbar\sigma_e^2}{\rho_c c_1^7} (\alpha^2 + \beta^2),$$

and

$$R_\sigma^{(\text{P},s)}(\omega) = R_{\sigma 0}^{(\text{P},s)} \omega^3 [n_B(\omega) + 1], \quad (\text{C5})$$

where

$$R_{\sigma 0}^{(\text{P},s)} = \frac{\gamma_s}{\pi^2} \frac{(g\mu_B B)^2}{(\hbar\omega_0)^4} \frac{\hbar}{\rho_c c_s^5} \left( \frac{de}{\epsilon_0 \epsilon_s} \right)^2 (\alpha^2 + \beta^2),$$

with  $\gamma_1 = 1/35$ ,  $\gamma_{t_1} = \gamma_{t_2} = 2/105$ . In the frequency range typical for the Zeeman energies in GaAs at moderate magnetic fields ( $\sim 0.1$  meV) the piezoelectric coupling to transverse modes dominates.

In the high-frequency region, where the deformation potential coupling dominates, we find the asymptotic estimate

$$\begin{aligned} R_\sigma^{(\text{DP})}(\omega) &= \frac{1}{4\pi^2} \frac{(g\mu_B B)^2}{(\hbar\omega_0)^4} \frac{\hbar\sigma_e^2}{\rho_c c_1^3} (\alpha^2 + \beta^2) \\ &\times [n_B(\omega) + 1] e^{-\frac{1}{2} \left( \frac{\omega l_z}{c_1} \right)^2} \frac{\omega}{(l_\perp^2 - l_z^2)^2}. \end{aligned} \quad (\text{C6})$$

The spectral function  $S_\sigma(\omega)$ , pertaining to the driven evolution of the system, depends in a complicated way on the performed qubit rotation and on the initial state. In order to reduce the complexity, we restrict the discussion to a  $\pi/2$  qubit rotation around the  $\sigma_x$  axis, i.e.  $\chi = \pi/4$ ,  $\delta_1 = 0$ . We parameterize the general initial qubit state in the form (31) and calculate the spin-flip contributions to the error averaged over the Bloch sphere of initial states. We will restrict the discussion to the most interesting high-frequency regime of operation, where the following hierarchy of time scales may be assumed:  $t_0 \gg \hbar/E_Z \gg t_1 \gg \tau_0$ .

Under these simplifying assumptions and neglecting terms proportional to  $E_Z \tau_0$  the first contribution to the spectral function  $S_\sigma(\omega)$  [Eq. (C3)] is

$$\begin{aligned} |\langle 0 | Y_\sigma(\omega) | 1 \rangle|^2 &\approx \\ &\frac{2\pi}{3} (2t_0 - 2t_1) [\delta(\omega + E_Z/\hbar) + \delta(\omega - E_Z/\hbar)] \\ &+ \frac{1}{\omega^2} |s_1(\omega)|_{\text{av}}^2, \end{aligned}$$

where ‘av’ denotes averaging over the Bloch sphere of initial states, as in Eq. (44). The first contribution leads to the Markovian (Fermi Golden Rule) spin-flip probability over the time  $2t_0 - 2t_1$  during which the electron is located in the first (‘‘large’’) dot, up to the factor  $1/3$  resulting from averaging of the spin-flip rates for various superposition states. The probability of such a process in a self-assembled quantum dot is extremely low due to large confinement energy. Indeed, the spin-flip rate



pertaining to this contribution is, according to Eq. (C2),

$$\begin{aligned} w &= \frac{2\pi}{3} [R_\sigma(E_Z/\hbar) + R_\sigma(-E_Z/\hbar)] \\ &\approx \frac{1}{3} \frac{16}{105\pi} \left( \frac{g\mu_B B}{\hbar\omega_0} \right)^4 k_B T \frac{1}{\hbar^2 \rho_c c_t^2} \left( \frac{de}{\varepsilon_0 \varepsilon_s} \right)^2 (\alpha^2 + \beta^2) \\ &= 1.0 \cdot 10^{-4} \text{ s}^{-1}, \end{aligned} \quad (\text{C7})$$

where we used the low-frequency formula (C5) for the spectral density (the piezoelectric coupling to transverse phonons dominates in this sector), substituted the Zeeman energy  $E_Z = g\mu_B B$  and assumed that  $k_B T > E_Z$ . The final value corresponds to  $T = 1$  K and  $B = 1$  T.

The other term describes an additional contribution to the spin-flip transition closely related to the pure dephasing effect [Eq. (41)]. Since the low-frequency behavior of the spectral densities for direct and SO-induced processes [Eqs. (A3) and (C5)] is the same, the ratio between the SO effect and the direct pure dephasing is

$$\frac{\delta_\sigma^{(1)}}{\delta^{(\text{pd})}} = \frac{R_{\sigma 0}^{(\text{P,t})}}{R_0^{(\text{P,t})}} = \frac{\hbar^2 (\alpha^2 + \beta^2) (g\mu_B B)^2}{D^2 (\hbar\omega_0)^4} = 1.7 \cdot 10^{-12},$$

where we included again only the dominating contribution from the piezoelectric coupling to transverse phonons. It is clear that the SO-related process is negligible compared to the pure dephasing.

Under the same assumptions as above, we have for the two other SO-induced contributions

$$|\langle 2, 3 | Y(\omega) | \psi_0 \rangle|_{\text{av}}^2 = \frac{1}{\omega^2} |s_{2,3}(\omega)|^2.$$

As discussed in Sec. V, the functions  $s_{2,3}(\omega)$  are relatively sharply peaked around  $\omega = -\lambda_\mp$ . Since the latter values are large, we use the high-frequency asymptotics for the spectral density (now the deformation potential coupling to longitudinal phonons dominates) and the ratio between the SO-related process and the transitions described in Sec. V may be written as

$$\begin{aligned} \frac{\delta_\sigma^{(2,3)}}{\delta^{(2,3)}} &= \frac{R_\sigma^{(\text{DP})}(-\lambda_\mp)}{R^{(\text{DP})}(-\lambda_\mp)} \\ &= \frac{(g\mu_B B)^2}{(\hbar\omega_0)^4} \frac{\hbar^2}{D^2 c_1^2} \lambda_\mp^2 (l_\perp^2 - l_z^2) (\alpha^2 + \beta^2), \end{aligned}$$

where we used the asymptotic formula (A4) since the optimal pulse parameters correspond to  $\lambda_\mp$  in a local minimum of the spectral density. For the parameter area

1 [cf. Fig. 3], i.e.  $\lambda_- = 12$  ps<sup>-1</sup>, one finds

$$\frac{\delta_\sigma^{(2)}}{\delta^{(2)}} = 1.8 \cdot 10^{-10}.$$

Again, the SO-related process is many orders of magnitude weaker than the transition discussed in the paper.

Apart from these contributions there is another one, to the spin-flipped state  $|2'\rangle$  in the small dot. This process is not possible in the absence of the SO coupling. The relevant spectral function is

$$\begin{aligned} |\langle 2' | Y(\omega) | \psi_0 \rangle|_{\text{av}}^2 &= \\ &= 2 \frac{\sin^2[(\omega - E_Z/\hbar)t_1 + g(\omega)]}{(\omega - E_Z/\hbar)^2} h^2(\omega - E_Z/\hbar), \end{aligned}$$

where we denoted

$$\int dt \cos \theta \dot{\theta} e^{i\omega t} = e^{ig(\omega)} h(\omega).$$

One has for the STIRAP transfer  $g(0) = 0$ ,  $h(0) = -1$ . The width of  $h(\omega)$  is of the order of  $1/\tau_0$ . For large  $t_1$  (long dwelling time in the small dot), this yields the spin-flip transition rate according to the Fermi Golden Rule, analogous to Eq. (C7) up to an averaging-related factor. For typical dwelling times  $\sim 100$  ps this would produce a negligible contribution to the error of order of  $10^{-14}$  for  $B \sim 1$  T,  $T \sim 1$  K. However, under the assumptions made above the FGR is not applicable; instead one may approximate

$$|\langle 2' | Y(\omega) | \psi_0 \rangle|_{\text{av}}^2 \approx \frac{1}{\omega^2} h^2(\omega).$$

Using the low-frequency and high-temperature approximation to  $R_\sigma^{(\text{P,t})}(\omega)$  one finds

$$\delta_\sigma^{(2')} \sim \left[ R_{\sigma 0}^{(\text{P,t}_1)} + R_{\sigma 0}^{(\text{P,t}_2)} \right] \frac{k_B T}{\hbar} \frac{1}{\tau_0} \sim 10^{-14},$$

at  $B \sim 1$  T,  $T \sim 1$  K. Note that under the conditions assumed here, the dominating contribution comes from the dynamical effect characterized by the inverse pulse duration  $1/\tau_0$ .

In conclusion, the Markovian spin-flip rate for a self-assembled QD with typical level separation is very long while dynamical effects involving the SO coupling remain in a fixed relation to those induced by direct phonon coupling and are negligible in comparison to them.

\* Electronic address: Pawel.Machnikowski@pwr.wroc.pl

<sup>1</sup> *The Physics of Quantum Information*, edited by D. Bouwmeester, A. Eckert, and A. Zeilinger (Springer-Verlag, Berlin Heidelberg, 2000).

<sup>2</sup> L. Jacak, P. Hawrylak, and A. Wojs, *Quantum Dots*

(Springer Verlag, Berlin, 1998).

<sup>3</sup> R. Hanson, B. Witkamp, L. M. K. Vandersypen, L. Willems van Beveren, J. M. Elzerman, and L. P. Kouwenhoven, *Phys. Rev. Lett.* **91**, 196802 (2003).

<sup>4</sup> D. Loss and D. P. DiVincenzo, *Phys. Rev. A* **57**, 120

- (1998).
- <sup>5</sup> T. H. Stievater, X. Li, D. G. Steel, D. Gammon, D. S. Katzer, D. Park, C. Piermarocchi, and L. J. Sham, *Phys. Rev. Lett.* **87**, 133603 (2001).
  - <sup>6</sup> H. Kamada, H. Gotoh, J. Temmyo, T. Takagahara, and H. Ando, *Phys. Rev. Lett.* **87**, 246401 (2001).
  - <sup>7</sup> H. Htoon, T. Takagahara, D. Kulik, O. Baklenov, A. L. Holmes Jr., and C. K. Shih, *Phys. Rev. Lett.* **88**, 087401 (2002).
  - <sup>8</sup> A. Zrenner, E. Beham, S. Stuffer, F. Findeis, M. Bichler, and G. Abstreiter, *Nature* **418**, 612 (2002).
  - <sup>9</sup> P. Borri, W. Langbein, S. Schneider, U. Woggon, R. L. Sellin, D. Ouyang, and D. Bimberg, *Phys. Rev. B* **66**, 081306 (2002).
  - <sup>10</sup> X. Li, Y. W. D. Steel, D. Gammon, T. Stievater, D. Katzer, D. Park, C. Piermarocchi, and L. Sham, *Science* **301**, 809 (2003).
  - <sup>11</sup> E. Biolatti, R. C. Iotti, P. Zanardi, and F. Rossi, *Phys. Rev. Lett.* **85**, 5647 (2000).
  - <sup>12</sup> P. Borri, W. Langbein, S. Schneider, U. Woggon, R. L. Sellin, D. Ouyang, and D. Bimberg, *Phys. Rev. Lett.* **87**, 157401 (2001).
  - <sup>13</sup> M. Bayer and A. Forchel, *Phys. Rev. B* **65**, 041308 (2002).
  - <sup>14</sup> E. Pazy, E. Biolatti, T. Calarco, I. D'Amico, P. Zanardi, F. Rossi, and P. Zoller, *Europhys. Lett.* **62**, 175 (2003).
  - <sup>15</sup> T. Calarco, A. Datta, P. Fedichev, E. Pazy, and P. Zoller, *Phys. Rev. A* **68**, 12310 (2003).
  - <sup>16</sup> A. Imamoglu, D. D. Awschalom, G. Burkard, D. P. DiVincenzo, D. Loss, M. Sherwin, and A. Small, *Phys. Rev. Lett.* **83**, 4204 (1999).
  - <sup>17</sup> M. Feng, I. D'Amico, P. Zanardi, and F. Rossi, *Phys. Rev. A* **67**, 014306 (2003).
  - <sup>18</sup> F. Troiani, E. Molinari, and U. Hohenester, *Phys. Rev. Lett.* **90**, 206802 (2003).
  - <sup>19</sup> U. Hohenester, F. Troiani, E. Molinari, G. Panzarini, and C. Macchiavello, *Appl. Phys. Lett.* **77**, 1864 (2000).
  - <sup>20</sup> Pochung Chen, C. Piermarocchi, L. J. Sham, D. Gammon, and D. G. Steel, *Phys. Rev. B* **69**, 075320 (2004).
  - <sup>21</sup> Z. Kis and F. Renzoni, *Phys. Rev. A* **65**, 032318 (2002).
  - <sup>22</sup> K. Bergmann, H. Teuer, and B. W. Shore, *Rev. Mod. Phys.* **70**, 1003 (1998).
  - <sup>23</sup> H.-P. Breuer and F. Petruccione, *The Theory of Open Quantum Systems* (Oxford University Press, Oxford, 2002).
  - <sup>24</sup> B. Krummheuer, V. M. Axt, and T. Kuhn, *Phys. Rev. B* **65**, 195313 (2002).
  - <sup>25</sup> A. Vagov, V. M. Axt, and T. Kuhn, *Phys. Rev. B* **66**, 165312 (2002).
  - <sup>26</sup> L. Jacak, P. Machnikowski, J. Krasnyj, and P. Zoller, *Eur. Phys. J. D* **22**, 319 (2003).
  - <sup>27</sup> A. Vagov, V. M. Axt, and T. Kuhn, *Phys. Rev. B* **67**, 115338 (2003).
  - <sup>28</sup> A. Vagov, V. M. Axt, T. Kuhn, W. Langbein, P. Borri, and U. Woggon, *Phys. Rev. B* **70**, 201305(R) (2004).
  - <sup>29</sup> R. Alicki, M. Horodecki, P. Horodecki, R. Horodecki, L. Jacak, and P. Machnikowski, *Phys. Rev. A* **70**, 010501(R) (2004), quant-ph/0302058.
  - <sup>30</sup> R. Alicki, M. Horodecki, P. Horodecki, and R. Horodecki, *Phys. Rev. A* **65**, 062101 (2002), quant-ph/0105115.
  - <sup>31</sup> C. Cohen-Tannoudji, J. Dupont-Roc, and G. Grynberg, *Atom-Phonon Interactions* (Wiley-Interscience, New York, 1998).
  - <sup>32</sup> G. D. Mahan, *Many-Particle Physics* (Kluwer, New York, 2000).
  - <sup>33</sup> G. D. Mahan, in *Polarons in Ionic Crystals and Polar Semiconductors*, edited by J. T. Devreese (North-Holland, Amsterdam, 1972).
  - <sup>34</sup> A. Messiah, *Quantum Mechanics* (North-Holland, Amsterdam, 1966).
  - <sup>35</sup> M. I. Dyakonov and V. I. Perel, *Sov. Phys.-Solid State* **13**, 3023 (1972), [*Fiz. Tv. Tela* **13**, 3581 (1971)].
  - <sup>36</sup> M. I. Dyakonov and V. Y. Kachorovskii, *Sov. Phys. Semicond.* **20**, 110 (1986), [*Fiz. Tekh. Poluprovodn.* **20**, 178 (1986)].
  - <sup>37</sup> U. Rössler, *Phys. Stat. Sol. (b)* **234**, 385 (2002).
  - <sup>38</sup> V. N. Golovach, A. Khaetskii, and D. Loss, *Phys. Rev. Lett.* **93**, 016601 (2004).
  - <sup>39</sup> A. V. Khaetskii, D. Loss, and L. Glazman, *Phys. Rev. Lett.* **88**, 186802 (2002).
  - <sup>40</sup> S. Adachi, *J. Appl. Phys.* **58**, R1 (1985).
  - <sup>41</sup> D. Strauch and B. Dorner, *J. Phys: Cond. Matt.* **2**, 1457 (1990).
  - <sup>42</sup> M. Kroutvar, Y. Ducommun, D. Heiss, M. Bichler, D. Schuh, G. Abstreiter, and J. J. Finley, *Nature* **432**, 81 (2004).